https://doi.org/10.5194/egusphere-2026-6674
Preprint. Discussion started: 13 November 2026
© Author(s) 2026. CC BY 4.0 License.

Beyond blocking anticyclones: Iberian cut-off lows amplified early season heat in UK and France 2026

Maeve Mayer[1,2,3,4,5], Paolo Chevalier[3,4], Belinda Hotz[6], Robin Noyelle[6], Soulivanh Thao[3,4], Claire Petter[1], and Pascal Yiou[3,4]

[1]Autorité de Sûreté Nucléaire et de Radioprotection (ASNR), DERT-SCAN-BEHRIG, F-92260, Fontenay aux Roses, 10587, France
[2]Electricité de France (EDF R& D), 7, boulevard Gaspard Monge, Palaiseau, 91120, France
[3]Laboratoire des Sciences du Climat et de l'Environnement (LSCE), CEA, CNRS, UVSQ, Université Paris-Saclay, CEA Orme des Merisiers, Gif-sur-Yvette, 91120, France
[4]Institut Pierre-Simon Laplace, Université de Versailles Saint-Quentin en Yvelines, Guyancourt, 78, France
[5]University of Hamburg, Bundesstraße 57, Hamburg, 20146, Germany
[6]Institute for Atmospheric and Climate Science, ETH Zürich, Universitätsstrasse 16, Zürich, 8092, Switzerland

Correspondence: Maeve Mayer (maeve.mayer@lsce.ipsl.fr)

Abstract. In May 2026, France and the United Kingdom experienced a record-breaking hot event with daily maximum temperature anomalies exceeding 15°C. Here, we show that the unprecedented high-pressure system over the region was insufficient to explain the full magnitude of near-surface temperatures in Western France and Southern UK. Using perturbed large ensemble medium-range forecasts from the IFS and AIFS models, we estimate that Iberian cut-off low activity explains about 30% of the additional temperature variance during the heatwave peak, conditional on the presence of the anticyclone. This contributed a local surplus of up to 4.5°C to daily mean surface temperatures compared to ensemble members that achieved similar 500 hPa geopotential height records. Across similar past synoptic events, we find a comparable impact of cut-off low activity, localized over the French Atlantic coast and southern UK. At the mid-tropospheric level, cut-off low activity drives advective warming from a Saharan branch. In a second stage, the arriving end of this branch is coupled to the boundary layer by increasing subsidence near 850 hPa. While this large-scale circulation pattern is highly unusual for May — being typically associated with late-summer warm spells — the Saharan branch reached an unprecedented southward extent during this event. Furthermore, while no dynamical trend was found for the month of May, June has shown a positive trend in Iberian cut-off low activity since 1985, characterized by a doubling in the occurrence of exceptionally intense cut-off lows. Our findings underscore the importance of cut-off low dynamics in driving extreme early-season heatwaves, a factor that is rarely quantified in previous analyses.

1 Introduction

Anthropogenic climate change has expanded the length of the mid-latitude summer season, which already allows for an earlier onset of extreme heat during May and June (Ivanovich et al., 2026; Xu et al., 2026; Scott et al., 2026). While heatwaves are in general known as extreme weather events causing severe impacts, most pronouncedly on human health (Kovats and

https://doi.org/10.5194/egusphere-2026-6674
Preprint. Discussion started: 13 November 2026
© Author(s) 2026. CC BY 4.0 License.

Kristie, 2006; Gasparrini et al., 2015; Ebi et al., 2021), early season heat in particular can overwhelm societies if it meets an unprepared public infrastructure. The May 2026 heat event in Western Europe occurred after two weeks of perturbed atmospheric conditions with cool and wet weather. This summer-like event took local authorities by surprise, as it occurred during a period when schools are open and economic sectors (including agriculture and construction) are active. The short and long-term effects of this event on society and ecosystems are still being evaluated. It was the first of a series of heat events during the European summer.

Météo-France showed that this event broke record values for any month of May since 1950 (corresponding to the start of homogeneous observations over France) (Météo France, 2026a). The maximum of the mean daily temperature value in May over Ile-de-France (Paris region) reached a record value, and exceeded the previous record by $\approx 1\,^{\circ}\mathrm{C}$ (Météo France, 2026a). Summer-like temperatures were observed, with daily maxima exceeding $38\,^{\circ}\mathrm{C}$ in various parts of France. This was probably not the hottest month of May since the beginning of the 20th century, as higher temperatures were recorded in the North of France during May 1944 (Séchet, 2004; Holliday et al., 2026), but the quality control of measurements at that time hinders a precise quantitative comparison.

Large-scale atmospheric conditions are the major driver contributing to the formation of hot surface temperatures on weekly to sub-weekly timescales (Domeisen et al., 2022). In mid-latitude summers, high pressure systems are a requirement for the formation of heatwaves (Barriopedro et al., 2023). Extreme high pressure conditions are typically associated with the formation of an anticyclone at upper and mid tropospheric levels, which is either embedded in a subtropical ridge or blocking of the upper level jet (Pfahl and Wernli, 2012; Woollings et al., 2018). Such blocking patterns can result from the breaking of strongly amplified Rossby waves (Woollings et al., 2018; Wang et al., 2026) and in extreme cases, the positive potential vorticity intrusion is detached from its southward origin, leading to closed positive geopotential height contours over the heatwave region (Woollings et al., 2018). The resulting anticyclone is then anchored between an upstream and a downstream depression, a structure typically referred to as an Omega-block. These depressions can lock the anticyclone in place as they influence the jet stream entry and exit (Hotz et al., 2024; Ezber et al., 2026).

The coupling of upstream depressions with downstream anticyclones over Western Europe has been a subject of increased interest in recent years (Vautard et al., 2023; D'Andrea et al., 2024; González-Alemán et al., 2026). In particular cases, these upstream depressions can detach from the jet stream, leading to the rapid formation of a cut-off low structure over or close to the Iberian peninsula. The meteorological conditions of the May 2026 event corresponded to such an Omega-blocking system (Fig. 1a), which led to high pressures over France. The geopotential height at 500 hPa (Z_{500}) even broke the 80-year record. Similarly, it was accompanied by a cut-off low over the Iberian Peninsula, that detached from a large depression around Iceland.

Such combinations of strong anticyclonic conditions coupled with an Iberian cut-off low structure have been observed in trajectories of most extreme heatwave events in Western Europe, namely in centennial preindustrial climate simulations (Noyelle et al., 2023a), rare event algorithm simulations (Lancelin et al., 2026) and in recent record-shattering events, such as the July 2022 (Ezber et al., 2026) and the June 2026 heatwave (Ionita and Nagavciuc, 2026). They have further been mentioned as contributor to persistent warm spells in South-Western Europe (Pappert et al., 2025), and driver of compound heat and rainfall extremes (Mittermeier et al., 2026). While some case studies consider the effect of cut-off lows implicitly

https://doi.org/10.5194/egusphere-2026-6674
Preprint. Discussion started: 13 November 2026
© Author(s) 2026. CC BY 4.0 License.

and show a general co-occurrence with Saharan Air intrusions and atmospheric deserts (Sousa et al., 2019; Fix et al., 2024; Fix-Hewitt et al., 2026), as well as their role in anchoring the anticyclone during the heatwave peak (Ezber et al., 2026), a detailed physical understanding of how cut-off lows impact heatwaves in western Europe is missing. In the face of a projected increase in mid-latitude cut-off low activity (Muñoz et al., 2020; Mishra et al., 2025), we here address how Iberian cut-off lows directly impact near surface temperatures in interaction with the anticyclone and how such impact can be quantified.

Following the rainy first two weeks of May, the May 2026 heat event installed the premises of a historically hot summer in France (Météo France, 2026b), despite high specific humidity during the heatwave peak (Fig. 1d). Summer temperatures peaked during June 2026, induced by a recurrence of high pressure and cut-off lows. Understanding how atmospheric conditions combined to generate the May heat event is useful for early warning of summer extreme heatwaves. Ensemble weather forecasts did not systematically lead to concomitant Omega blocks and cut-off lows. The AIFS system from the European Centre for Medium-Range Weather Forecasts (ECMWF) (Lang et al., 2026) provides a unique opportunity to investigate the respective roles of the anticyclonic and cut-off low conditions in a consistent manner, i.e., from the same atmospheric initial conditions.

The scientific question of the manuscript is to quantify the contribution of the physical mechanisms that lead to summer-like temperatures in May, in France and Southern UK. We employ an ensemble of weather forecast simulations with the IFS (ECMWF, 2026) and AIFS-ENS models (Lang et al., 2026) as well as synoptic analogues (Jézéquel et al., 2018) from ERA5 reanalysis (Soci et al., 2024). This analysis of the atmospheric dynamics allows determining whether the extreme heat was linked to the unusual interaction of usual patterns. To understand the thermal features of those atmospheric patterns, we apply a Lagrangian heat decomposition to IFS and synoptic analogues (Röthlisberger and Papritz, 2023), which allows identifying the sources of heat that reached France and the UK, especially during the cut-off low occurrence.

The data (reanalyses and ensemble forecast) and methods (Lagrangian decomposition, cut-off low detection and analogues) are described in Sec. 2. Results for the analyses of the May heatwave are discussed in Sec. 3. We briefly discuss implications for other heatwave events in Sec. 4. Conclusions are drawn in Sec. 5.

2 Data and Methods

2.1 Reanalysis and ensemble forecast data

We first use the ERA5 atmospheric reanalysis from January 1940 to August 2026 (Copernicus Climate Change Service, 2023; Soci et al., 2024) to diagnose the atmospheric features of the May 2026 event. The original $0.25° \times 0.25°$ resolution is used for all May maximum temperature (TXx, monthly maximum of the daily maximum) analyses and variables at time of TXx, computed as the monthly near surface temperature maximum from hourly resolution for each grid cell for each Month of May between 1940 and 2026. The daily mean Z_{500} fields of ERA5 are bilinearly regridded from the original ERA5 Gaussian grid to a regular global $1 \times 1°$ grid. Cut-off low detection and circulation analogues are determined on fields with this coarse resolution. We use a horizontal resolution $0.5° \times 0.5°$ for daily mean surface temperature analysis and Lagrangian tracing, as adapted from Röthlisberger and Papritz (2023).

https://doi.org/10.5194/egusphere-2026-6674
Preprint. Discussion started: 13 November 2026
© Author(s) 2026. CC BY 4.0 License.

ECMWF's Integrated Forecasting System (IFS) archive data for 2026 is used to investigate alternative meteorological trajectories that could have been obtained in May 2026. 50 members of the IFS ensemble forecasts for geopotential height on pressure levels and near surface temperature are provided by ECMWF and were obtained from the ECMWF Data Store under the TIGGE license (Bougeault et al., 2010; ECMWF, 2026; ECMWF Data Store Service, 2026). IFS daily means are computed on 6 hourly outputs and bilinearly regridded to be consistent with ERA5. For the Lagrangian decomposition, the IFS runs on model levels were separately obtained from MeteoSwiss and ECMWF. We cross-verified the member indexing with the TIGGE Archive by comparing 12 UTC near surface temperatures for each member and initialization for the valid date of the 25th of May 2026 over Western Europe. Throughout the manuscript we refer to several regions to derive drivers, impact and causality which are all together visualized in Supplement Figure S1 and explained throughout the following section.

We consider a fixed rectangular box including the South of UK and Western France anchored between 44.5°N–5.5°W and 55°N–5°E as the region of strongest temperature anomalies during the May 2026 heatwave, which is referred to as the UK-France region. Except for the Lagrangian decomposition, we use a consistent reference climatology from 1995 to 2025 computed from daily means, which are smoothed along a rolling and centered 7-day window around the selected day of year based on ERA5.

2.2 AIFS-Ens model simulations

This study uses the AIFS-Ens (v1) model (Lang et al., 2026) as an emulator of IFS in order to obtain ensembles with sufficient sizes to obtain statistically reliable composites with and without cut-off lows. The AIFS-Ens (v1) model is a data-driven weather forecasting system developed by the European Centre For Medium Range Weather Forecasting (ECMWF). It is trained on ECMWF's ERA5 reanalysis (Copernicus Climate Change Service, 2023) and fine-tuned with ECMWF's operational numerical weather prediction analyses up to 2023. It is trained to predict the state of the atmosphere at 6 hours time steps $X(t+6) = \mathrm{AIFS}\,(X(t), X(t-6))$. Locally, AIFS is initialized with ERA5 data at 0.25°, which was gridded to a N320 reduced Gaussian grid (Lang et al., 2026) to match the model grid. The model simulates output data on the same N320 grid, which we do not regrid to regular rectangular gridded data because regridding can be computationally expensive and it is easy to use the N320 grid for most analyses. The only task that needed regridding was the cut-off detection. The scorecards in Lang et al. (2026) show AIFS-CRPS ensemble forecasts are more skillful than the IFS ensemble for a number of variables, such as near surface temperature, or temperature at 850 hPa, which makes it relevant for our study. We also decided to use this model for its computational cost (a 20-day forecast using AIFS-Ens runs under two minutes on a single NVIDIA A100 GPU). AIFS-Ens is a probabilistic model, wherein the noise necessary to make ensemble predictions is introduced directly into the latent space. Therefore, given suitable initial conditions, this can generate as many independent ensemble predictions as needed, without having to use perturbed ensemble as initial conditions.

We simulate an ensemble of 201 simulations per initialization date of AIFS-Ens, with initial conditions on May 17th and 18th 2026 taken from ERA5 for reasons explained in Section 3.1.

https://doi.org/10.5194/egusphere-2026-6674
Preprint. Discussion started: 13 November 2026
© Author(s) 2026. CC BY 4.0 License.

2.3 Cut-off low detection and definition

We perform the cut-off low detection on daily mean Z_{500} fields using the MIT licensed `colindex2` module (Kasuga, 2022; Kasuga et al., 2021). For the detection of *Iberian cut-off lows*, we select cut-offs whose center is detected between 35°W to 0°W and 25°N to 50°N, with a broader predetection box edging with at least 20° to each direction (10° for AIFS due to storage constraints). The selection box broadly reflects a region in the East subtropical North Atlantic associated with frequent cut-off low occurrence during spring to summer, as highlighted throughout previous works using various methodologies for cut-off detection (Nieto et al., 2005; Portmann et al., 2021; Kasuga et al., 2021; Mishra et al., 2025). From the geometry of cut-off lows in geopotential height fields, Kasuga et al. (2021) introduce a measure of cut-off low intensity, the optimal Slope So, which reflects the maximum gradient of the depression. Here, we use a minimum optimal slope of $So > 6$ m per 100 km for detection. The further setup is detailed in Supplement Section S2.2.

We utilize the detection to introduce a binary classification of whether or not a forecast member features an Iberian cut-off low on the 25th of May or respective flow analogue date (as detailed below). The two resulting pools of members with and without Iberian cut-off low are referred to as *cut-off* and *no cut-off* pools for the respective experiment. To measure the effect of persistent Iberian cut-off low activity preceding the heatwave event, we detect the optimal Slope So for each forecast member between the 21st and the 25th of May (or, respectively, up to four days before the selected analogue date). The choice of five consecutive days is designed to capture persistence effects within the analogues, as five days is the upper end of cut-off low life-cycles (Nieto et al., 2005; Portmann et al., 2021), approximately the 90th Percentile in the mid latitudes at 500 hPa (Muñoz et al., 2020). The optimal Slope So is then summed over all these preceding days where an Iberian cut-off low is detected. We continue to refer to the resulting metric as *preceding cut-off low activity*. To make the preceding cut-off low activity metric more intuitive for the reader, we normalize by the daily mean Iberian cut-off low activity of $\overline{So} = 15$ m $(100\text{ km})^{-1}$. As preceding cut-off activity considers multiple consecutive days, while the binary classification relies on one day only, forecast ensemble members and analogue days belonging to the no cut-off pool can have preceding cut-off low activity larger than 0. However they account, by construction, for one day less of preceding cut-off low activity and are consequently expected to show less preceding cut-off activity than the cut-off pool on average.

2.4 Past Flow analogues

To compare the May 2026 heatwave with similar past synoptic events, we use the methodology of Noyelle et al. (2025) to select past flow analogues from ERA5. Based on the detrended daily mean 500 hPa geopotential height fields (Jézéquel et al., 2018), we select the N days with the smallest Euclidean distance between April to August in the years 1940 to 2025 in the region of [30–68°N; 20°W–25°E] (Supplement Figure S1). We apply an exclusion criterion of 5 days before and after the selected analogue date to avoid clustering. In cases where we divide cut-off and no cut-off analogue pools, each pool is selected from the same overall ranking, meaning the exclusion criterion is sustained between cut-off and no-cut-off pool.

To estimate the effect of cut-off low activity on near surface temperature in the present day climate (i.e. detrended), we linearly project the daily mean temperature anomaly to 2025 similar to Noyelle et al. (2025): the European regional mean

https://doi.org/10.5194/egusphere-2026-6674
Preprint. Discussion started: 13 November 2026
© Author(s) 2026. CC BY 4.0 License.

surface temperature (RMST) is computed as daily mean near surface temperature averaged over 35–70°N and 15°W–30°E, smoothed with a 15-year centred running mean. The first and last 7.5 years, which are not covered by the running mean, are extrapolated linearly from a fit to the first and last 30 years of the smoothed series. The UK-France box temperature anomaly T' at analogue day d with respect to the 1995–2025 reference climatology is projected linearly into the year 2025 following

$$T'_{2025}(d) = T'(d) + \beta_{RMSTA} \cdot [\mathrm{RMST}_{2025}(\text{25th May}) - \mathrm{RMST}(d)], \tag{1}$$

where the regression slope β_{RMSTA} is obtained from a linear fit of the UK-France box anomaly on RMST over all MJJA days between 1940 and 2025. The resulting target region warming rate is the same as the warming rate of RMST with a slope of 1.04 [0.97, 1.11] °C per °C RMST. We note that this computation of β_{RMSTA} is a methodological difference to Noyelle et al. (2025), who estimate the linear regression slope from within the analogue pool. We justify this choice as the bootstrap and regression procedure of Noyelle et al. (2025) to each pool of $N = 85$ analogues results in warming rates of 1.33 [0.46, 2.10] °C per °C RMST for the cut-off pool and 1.13 [0.61, 1.67] °C per °C RMST for the no cut-off pool, hence overlap with warming rates of the mean MJJA warming rate of the target region with much larger uncertainties. The number of $N = 85$ years is chosen in consistency with previous studies, using the order of one analogue per year (Jézéquel et al., 2018; Noyelle et al., 2025).

2.5 Z_{500}-control: Controlling near surface temperatures with respect to geopotential height

As we aim to explore what drove the May 2026 heatwave beyond the expected link of extreme geopotential height to near surface temperature, we compute the residuals of the regression of the daily mean surface temperature anomaly over the UK-France region on the Z_{500} anomaly over the same region. This is done as follows: The spatial average of daily mean near surface temperature anomaly is projected to the present day climate following equation 1. In the same way, we project the geopotential height anomaly at 500 hPa to the present day climate, i. e. we deseasonalize and then detrend:

$$Z'_{500,2025}(d) = Z'_{500}(d) + \beta_{RMSTZ} \cdot [\mathrm{RMST}_{2025}(\text{25th May}) - \mathrm{RMST}(d)], \tag{2}$$

with a slope of 19.24 [16.32, 22.13] m per °C of RMST obtained from ordinary least squares (OLS) regression. We then fit the OLS slope between Z'_{500} and the daily mean surface temperature both projected to the present day climate over all MJJA days from 1940 to 2025:

$$T'_{2025}(d) = \alpha + \beta_{ZT}\, Z'_{500,2025}(d) + \varepsilon(d), \tag{3}$$

with $\alpha = 0.4$ °C and $\beta_{ZT} = 0.0151\,[0.0148, 0.0154]$ °C per m fitted over all May to August days between 1940 and 2025. The detrended geopotential height anomaly $Z'_{500,2025}$ over the UK-France region explains about 50% of the variance of detrended near surface temperature anomalies $T'_{2025}(d)$. The Z_{500}-controlled temperature anomaly is obtained from the residual of this fit,

$$\widetilde{T}(d) = T'_{2025}(d) - \left[\alpha + \beta_{ZT}\, Z'_{500,2025}(d)\right]. \tag{4}$$

https://doi.org/10.5194/egusphere-2026-6674
Preprint. Discussion started: 13 November 2026
© Author(s) 2026. CC BY 4.0 License.

2.6 Lagrangian analysis of temperature anomalies

To quantify the processes leading to the high temperature anomalies, we use the temperature anomaly decomposition framework developed by Röthlisberger and Papritz (2023), based on the Lagrangian analysis tool LAGRANTO (Wernli and Davies, 1997; Sprenger and Wernli, 2015). Temperature anomalies (T') at the starting time of the trajectory x_f can be decomposed into a seasonality T', advective T', adiabatic T', and diabatic T' part:

$$\begin{aligned} T'(\boldsymbol{x}, t_f) = &- \int_{t_g}^{t_f} \frac{\partial T_{clim}}{\partial t}\, d\tau - \int_{t_g}^{t_f} \boldsymbol{v} \cdot \boldsymbol{\nabla}_{\mathrm{h}} T_{clim}\, d\tau \\ &+ \int_{t_g}^{t_f} \left[\frac{\kappa T}{p} - \frac{\partial T_{clim}}{\partial p} \right] \omega\, d\tau + \int_{t_g}^{t_f} \left(\frac{p}{p_0} \right)^{\kappa} \frac{D\theta}{Dt}\, d\tau, \end{aligned} \tag{5}$$

where t_g is last time that T' was zero, T_{clim} the climatological temperature, $\boldsymbol{v}$ the horizontal wind, $\boldsymbol{\nabla}_{\mathrm{h}}$ the horizontal gradient operator, $\kappa = \frac{R}{c_p}$, p the pressure and p_0 the reference pressure. The residual terms and the seasonality T' are usually small (Röthlisberger and Papritz, 2023) and are therefore neglected in the following.

To run temperature anomaly decomposition, we use a 6-hourly temporal and 0.5° horizontal resolution on the Northern Hemisphere. In order to run 15-day backward trajectories between the 18th May and 30th May, we combine the data of each IFS ensemble member with the operational analysis into a continuous time series from which the trajectories are started. The trajectories are started at each time step between 1000 hPa and 200 hPa with a spacing of 50 hPa. We trace pressure, temperature, climatological temperature (9-year and 21-day centered temperature mean), the change in the climatological temperature, the vertical change in the climatological temperature (difference in the climatological temperature 10 hPa above and below the trajectory), potential temperature, and the surface pressure. The exact computation of the reference climatology is detailed in (Hotz et al., 2024) and the computation of equation (5) in Röthlisberger and Papritz (2023). For the analysis of 2026, we use the same climatology as used for 2021 to 2025, i.e., the rolling 21-day mean over the years 2017 to 2025.

To reduce computational cost, IFS tracing runs on a cropped domain, spanning from 130 °W to 80 °E and 15 °N to 80 °N on the lowermost 68 hybrid sigma-pressure model levels (model level 70 to 137). ERA5 and analogues run on the entire Northern Hemisphere and all model levels. The main conclusions of this manuscript are expected to remain unchanged by the IFS domain limitation, as discussed in Supplement S3.2 together with the IFS Bias.

2.7 Air mass origin contribution maps

In this study, we introduce an air mass origin contribution analysis to attribute a final contribution of a Lagrangian temperature anomaly to the geographic origin of its trajectory. As in Papritz and Röthlisberger (2023), each trajectory i bears a genesis location $\mathbf{x}_{i,g}^{P}$, which marks the location along the trajectory of the latest sign change of each process P. Assuming $\Delta T_{i,f}^{P}$ is the final temperature anomaly contribution of process P for trajectory i at arrival time, $\Delta T_{i,f}^{P}$ is then mapped to its process genesis location $\mathbf{x}_{i,g}^{P}$ on a 0.5°×0.5° longitude×latitude grid. The final contribution of the considered process to the total temperature anomaly is retained for the process genesis grid cell. Aggregated over all trajectories arriving between pressure levels over

https://doi.org/10.5194/egusphere-2026-6674
Preprint. Discussion started: 13 November 2026
© Author(s) 2026. CC BY 4.0 License.

a given arrival time window, we normalize each resulting map by the total number of all arriving trajectories for the given pressure and arrival time band. We further introduce area weighting in units of 10^6 km^2 to generate physically meaningful and interpretable results in consistency with Papritz and Röthlisberger (2023). Put into mathematical terms, we assume N trajectories arrive in region Ω_f in a given arrival time window $[t_{0,f}, t_{1,f}]$ and arrival pressure band $[p_{0,f}, p_{1,f}]$. Of these N trajectories, a subpool $M \leq N$ will have their genesis of process P at location $\mathbf{x}^P_{i,g}$ in the 0.5°×0.5° grid cell $\mathcal{C}(\mathbf{x}^P_g)$, allowing for the final plotted contribution per grid cell to be expressed as:

$$S^P(\mathbf{x}^P_g) = \frac{1}{A(y)} \frac{1}{N} \sum_i \Delta T^P_{i,f} \, I\left[\mathbf{x}^P_{i,g} \in \mathcal{C}(\mathbf{x}^P_g)\right] \; I[t_{i,f} \in [t_{0,f}, t_{1,f}] \wedge p_{i,f} \in [p_{0,f}, p_{1,f}] \wedge \mathbf{x}_{i,f} \in \Omega_f\,],$$

with indicator function I and area weighting $A(y) = R^2 \, \Delta\lambda^2 \cos y$ in units of 10^6 km^2, R is Earth radius and $\Delta\lambda$ the mapped grid resolution. The resulting methodology hence differs from the source-sink framework introduced by Papritz and Röthlisberger (2023), which identifies gradual changes of the process contribution along the trajectory paths and iteratively scales them to temperature anomaly sources and sinks after genesis. Our contribution framework instead focuses on the origin of air-masses and their role to the final temperature anomaly contribution, emphasizing regions of temperature anomaly genesis instead of downstream sources and sinks. We note that only a third of advective contributions change sign further downstream (evaluated for May 2026, ERA5) so that the process genesis location coincides with the genesis location of the total temperature anomaly in most cases.

3 Results

High pressure anticyclonic conditions are very effective to increase surface temperatures, through increased subsidence and clear skies (Domeisen et al., 2022). Such an anticyclone is generated by a two-stage upper tropospheric process during the May 2026 heatwave: a strongly positive potential vorticity filament starts to dissipate downwards around the 18th to 19th of May and, as it does, deflects a part of the depression approaching Europe Northward (white filament at 50°N–25°W in Figure 2a). The deflection generates an atmospheric ridge on the 21st of May (Figure 2c,d), which is reinforced by an anticyclonic Rossby wave breaking approaching on the 23rd of May (Figure 2e,f). The second wave breaking event generates a potential vorticity filament that reaches deep into the troposphere over the North of Portugal (Figure 2f). The filament is entirely cut off from the jet stream at the 24th of May (Figure 2g), briefly maintaining its vertical depth (Figure 2h). The two sequential wave breaking events result in an exceptional 500 hPa geopotential height (Z_{500}) at the heatwave peak on the 25th of May 2026 (Figure 1a) paired with an Iberian cut-off low north of Portugal, a situation typically known as an Omega-block. We first show that the generation of this cut-off low increased the near-surface temperature response beyond the expected effect of the extreme Z_{500} value, by demonstrating that the record-breaking Z_{500} over western Europe is not alone sufficient to explain the observed record-breaking heat over Southern UK and Western France.

https://doi.org/10.5194/egusphere-2026-6674
Preprint. Discussion started: 13 November 2026
© Author(s) 2026. CC BY 4.0 License.

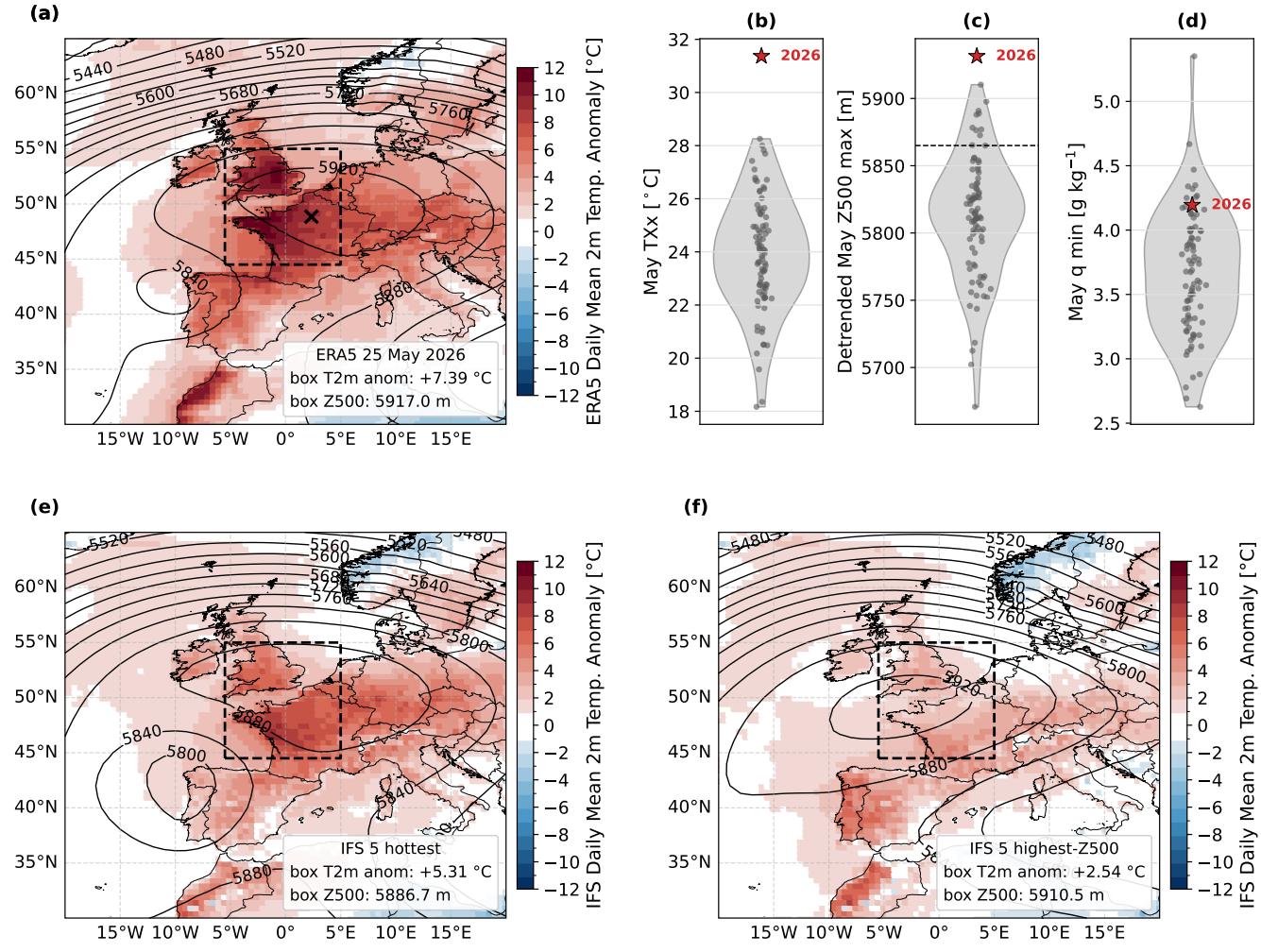


Figure 1. Overview of the May 2026 Western European Heatwave Characteristics. (a) ERA5 daily mean temperature anomaly on the 25th of May 2026 against 7-day smoothed climatology of 1995–2025. Isolines are for Z_{500}, with 40m increments. The region of most intense temperature anomalies (UK and France) is highlighted with a dashed box; the cross indicates Paris. (b) The ERA5 2026 May maximum temperature (TXx), (c) the highest May Z_{500} value, linearly detrended against yearly regional mean surface temperature of Europe and projected into the present day climate, (d) and minimum May near-surface moisture (red stars) are compared with previous May extreme states from 1940 to 2025 (grey dots), all averaged over land-only grid cells in the UK-France Box. (e) Daily mean near surface temperature anomaly (colours) and geopotential height field (contours) of composite from 5 IFS members with the highest daily mean near surface temperatures over the dashed UK-France region, selected across initialization from the 17th and 18th of May. (f) as (e), but top 5 composite selected from highest Z_{500} field, excluding members which feature in (e).

https://doi.org/10.5194/egusphere-2026-6674
Preprint. Discussion started: 13 November 2026
© Author(s) 2026. CC BY 4.0 License.

3.1 Atmospheric features of the event

We first consider the Z_{500} averaged over the UK-France target heatwave region (Box in Fig. 1a) in the 50 members perturbed IFS ensemble (Supplement Figure S3). The realized atmospheric block on the 25th of May 2026 is on the upper end of the predicted range of the Z_{500} IFS ensemble. To assess the forecast probability of reaching such a strong atmospheric ridge, we consider the previous (raw) daily mean Z_{500} May record over the UK-France region of 5860 m, dated to the 26th of May 2020. This threshold is about 55 m lower than the realization of the 25th of May 2026.

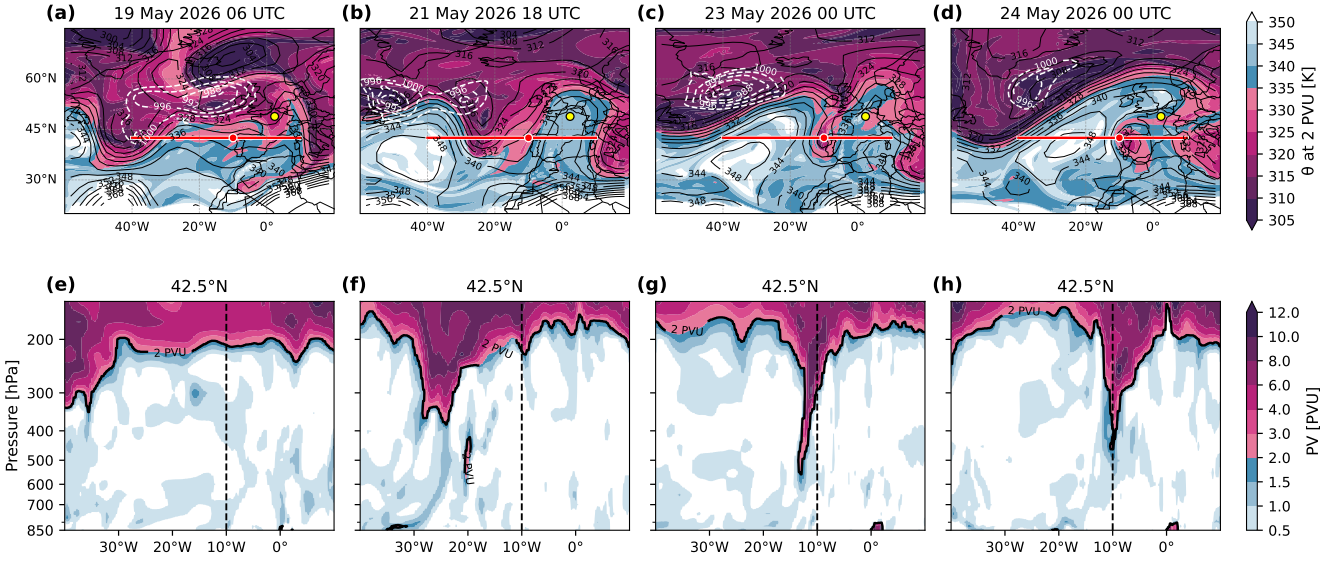


Figure 2. ERA5 Potential Vorticity Dynamics during May 2026 Heatwave Onset. (a-d) Potential temperature θ at 2 Potential Vorticity units (PVU) (colours), same field spectrally truncated at wavenumber 45 in 4K steps (black contour) and surface low pressure systems (mean sea level pressure below 1000 hPa, white in 4 hPa steps) at selected times between the 19th and the 24th of May 2026 (a-d). We highlight the longitudinal band for which we plot the longitudinal profile in (e-h) in red. (e-h) Vertical cross section of potential vorticity at 42.5°N with 2 PVU contour as black contour. The center of the generated cut-off low at 500 hPa as red dot / dashed vertical line and Paris as yellow dot.

A shift in forecast probability for meeting a Z_{500} threshold of 5860 m on the 25th of May occurs from the 18th to the 19th of May, with a change in predicted probability of more than 35% from one day to the next (Supplement Figure S3b). At the same time, the standard deviation in forecasted Z_{500} outcomes for the 25th of May rapidly decreases (Supplement Figure S3c). Consequently, we identify the 17th and 18th of May as a turning point for the predictability of a high Z_{500} value. The decline of forecast diversity and increased occurrence probability of the atmospheric block is associated with the more robustly predicted dipole system of a cut-off low over Portugal and a high-pressure system over the heatwave region (Supplement Figure S3d-f).

We use the identified initialization period between the 17th and 18th of May to probe the effect of high Z_{500} on the heatwave region at the 25th of May in Figure 1e–f. By pooling across both initialization dates, we form composites over two different constraints: the five members that forecast the hottest daily mean near surface temperatures over the UK-France region, and

https://doi.org/10.5194/egusphere-2026-6674
Preprint. Discussion started: 13 November 2026
© Author(s) 2026. CC BY 4.0 License.

the five members that have the highest regional mean Z_{500}. Only one member ranks in the top five of both, ranking fifth in the Z_{500} composite. We retain it in the temperature composite where it ranks higher and take the next-highest ranking member for the Z_{500} composite. These two members differ by $\Delta Z_{500} < 1$ m (and 2.3°C), so that the mean geopotential height of the top five Z_{500} composite stays effectively unchanged, while the temperature difference is shifted significantly. This leads to two non-intersecting subsets for which we compute composites. The maximum predicted Z_{500} in the geopotential height selected composite lies 30m above ERA5 on the 25th of May (Fig. 1f). However, these IFS members underestimate the observed daily mean temperature in the UK-France region by 4.8°C. The 5 hottest members over southern UK and France underestimate the daily mean near surface temperature on the 25th of May by only 2°C, but predict a weaker Z_{500} field on the 25th (Fig. 1e), with Z_{500} underestimations of ≈ 7 m. These hot members feature a pronounced cut-off over Spain, with a prediction of a deeper depression connected to an improved estimate of near-surface temperature.

In the following, we refer to members where we detect an Iberian cut-off low on the 25th of May as *cut-off* members. Conversely, we refer to forecast members for which no cut-off is detected as *no cut-off* forecast scenarios, as they feature a strong atmospheric block *without* a cut-off low feature on the 25th. We find that the 5 hottest members fall into the cut-off category, while the 5 highest Z_{500} members fall into the no cut-off category. In this framework, the cut-off members are slightly, but significantly, warmer than the no cut-off members considering the daily-mean surface temperature (ΔT2m $= +0.81\,$°C, Welch $p < 0.001$), and this difference strengthens when we control the effect of Z_{500} on the daily mean surface temperature, i.e., when we consider the residuals of the linear regression of near surface temperature on Z_{500} (ΔT2m $= +0.97\,$°C, Welch $p < 0.001$; Fig. 3a). We further observe that the preceding Iberian cut-off low activity amplifies near-surface temperatures when cut-off low activity is treated as a continuous quantity rather than a binary classification: Across the IFS large ensemble (50 per initialization, i.e. 100 selected members in total), preceding cut-off activity is only weakly correlated with the near-surface temperature (Pearson $r = 0.30$, Spearman $\rho = 0.31$, $p \approx 0.003$). However, the statistical link increases to a moderate but significant signal once the linear dependency of near surface temperature on Z_{500} is removed (hereafter the Z_{500}-controlled framework; see Method subsec. 2.5); Pearson $r = 0.55$, Spearman $\rho = 0.54$, $p < 0.001$). To further investigate the dependency of cut-off low activity with near-surface warming more systematically in a larger ensemble, we turn to the AIFS-Ens forecast ensemble.

3.2 Probing cut-off low impact with AIFS simulations

We consider an ensemble of 201 AIFS-Ens (Lang et al. (2026), see Sec. 2.2) simulations that are initialized on May 17th and 18th (predictability analysis of the atmospheric block in Supplement Figure S4). As AIFS has a large ensemble size, we decide for a Z_{500}-*matched* subselection, where we directly compare a large ensemble size with similarly high Z_{500}. To build the Z_{500}-matched pool each member is required to reach the $Z_{500} > 5860$ m threshold (previous May Z_{500} record) over the UK-France region on the 25th of May. Respectively 60% and 80% of the simulations reach the threshold 5860 m. Of all the AIFS simulations starting on the 17th and 18th, respectively 11 % and 53 % exceed a 18.7 °C daily mean temperature threshold in the 25th of May 2026, which is ERA5's 1940–2025 May maximum for the UK–France region. In IFS simulations initialized

https://doi.org/10.5194/egusphere-2026-6674
Preprint. Discussion started: 13 November 2026
© Author(s) 2026. CC BY 4.0 License.

on the same dates, 0 % and 10 % exceed the 18.7°C daily mean temperature threshold, underlining the performance of AIFS to simulate this particular event.

For a first comparison with IFS, we pull the 10 AIFS forecast members with the highest daily mean surface temperature on the 25th and the 10 AIFS members with highest Z_{500} pooled across both initialization dates. Remarkably, none of the AIFS members of the 10 hottest composite overlap with members of the top 10 Z_{500}. The 10 hottest AIFS members have a daily mean surface temperature 3.1°C warmer compared to the 10 highest Z_{500} composite. Conversely, the top 10 Z_{500} AIFS composite has a stronger geopotential height of 20 m. This is related to the same atmospheric features as before, as can be seen in Supplement Figure S5.

To verify the cut-off low amplification of near-surface temperatures over France and UK present in AIFS, we sort the Z_{500}-matched members into cut-off and no cut-off members, targeting the 25th of May (see Figure 3). The results are consistent with IFS results: over the UK-France region the cut-off members have a temperature average of ≈ 1.3°C warmer than the no cut-off members (Welch p <0.01, Figure 3b). The presence of a cut-off low on the 25th of May increases the probability of reaching the observed UK-France daily mean temperature anomaly of 7.4°C from $\approx 0.7\%$ to $\approx 4.5\%$ (estimated from the skew-normal fits in Figure 3 b). Preceding cut-off low activity explains about 30% of the variance in daily mean near surface temperature on the 25th of May 2026 within the Z_{500}-matched sub-selection (Pearson $r = 0.55$, Spearman $\rho = 0.63$, $p < 0.001$).

We investigate the impact of the Iberian cut-off low by selecting the 10 members from the AIFS simulations for each initialization date with the highest preceding cut-off low activity from the Z_{500}-matched cut-off sub-ensemble. From this, we obtain a third composite, which we compare against the entire Z_{500}-matched subselection, cut-off and no cut-off pooled (Figure 3c-e). Significant warming occurs in areas that experienced the highest temperature anomalies in May 2026: The French Atlantic Coast and Southern UK. The warming occurs within the high pressure system, most pronounced on the interface between the cut-off low and the anticyclone (for the initialization of the 18th; Figure 3e). Further warming occurs on the Western flank of the anticyclone (Init 17th; Fig 3c). In significantly impacted areas of the UK-France region, these members with the highest preceding cut-off low activity forecast an additional average warming of 1.7°C compared to the Z_{500}-matched ensemble mean. The top 5% most severely affected grid-points experienced excess warming of 3.5°C solely due to the presence of the cut-off, peaking at 4.5°C excess in the most impacted grid-points. The largest significant difference in vertical temperature structure induced by the cut-off low over the UK-France region takes place at the surface and lower troposphere after a warming throughout the entire atmospheric column at the heatwave start (Fig. 3d,f). As altitude increases, the difference is reduced, crossing 0 between 500h Pa and 800 hPa at the heatwave peak depending on the initialization date. The highest cut-off low activity composite shows that high temperatures in the case of the May 2026 heatwave are driven by the combination of two synoptic patterns: a record breaking blocking and a cut-off low west of the Iberian peninsula.

3.3 Reproducibility of cut-off low amplification in synoptic flow analogues

So far we have shown that the existence and preceding persistence of an Iberian cut-off low impacted the amplitude of the May 2026 heatwave in the UK-France region, especially where record breaking temperatures were registered. In this section, we

https://doi.org/10.5194/egusphere-2026-6674
Preprint. Discussion started: 13 November 2026
© Author(s) 2026. CC BY 4.0 License.

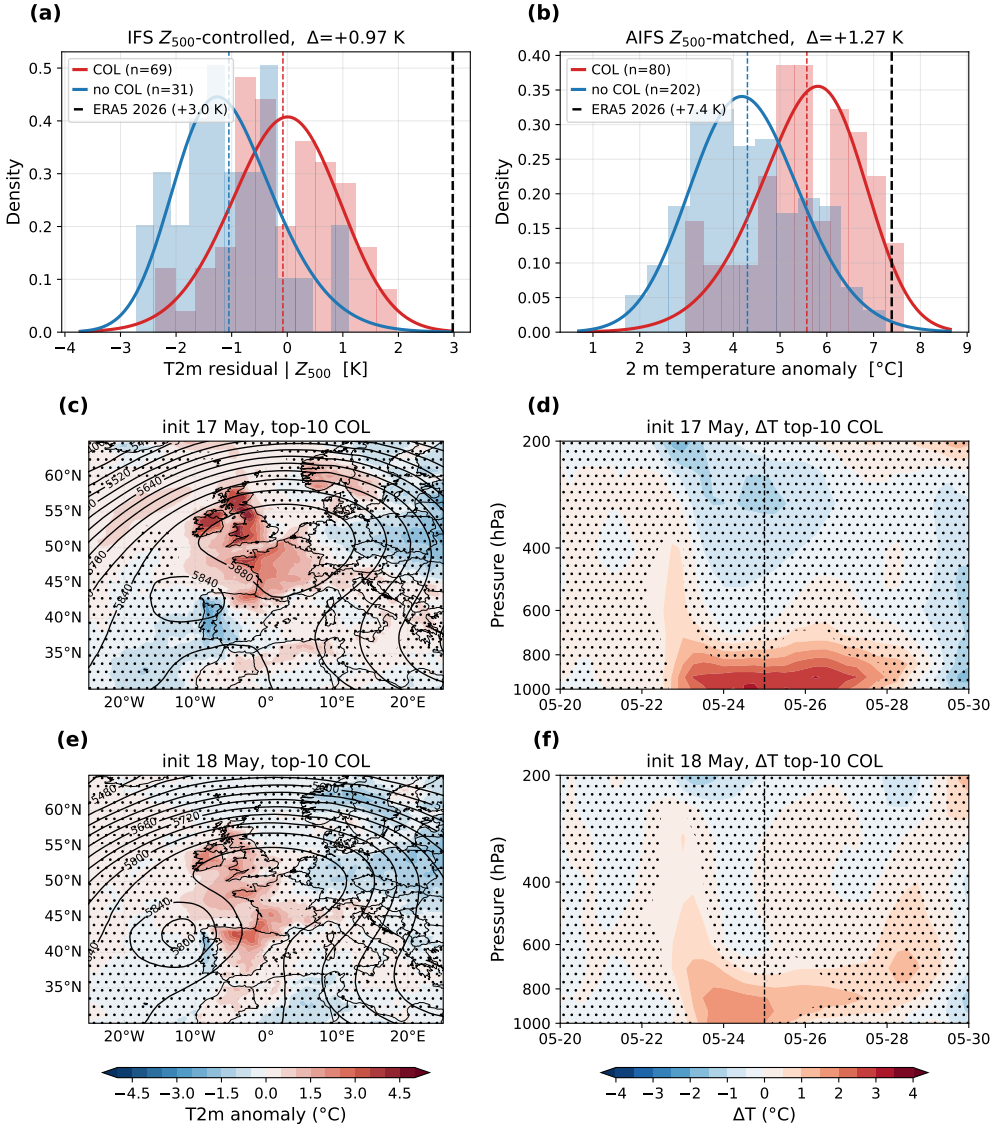


Figure 3. Effect of Iberian Cut-Off Low Activity on 25th of May temperatures in IFS and AIFS Perturbed Forecasts. (a) Residual of predicted daily mean near surface temperature after Z_{500}-control for the pooled IFS initializations of the 17th and 18th of May. Members with Iberian Cut-off on the 25th of May in red, members without in blue. (b) Predicted daily mean surface temperature anomalies in AIFS with same color coding (only upstream cut-off lows classify as Iberian cut-off low), using all members exceeding the threshold $Z_{500} > 5860$ m instead of removing the dependency on Z_{500}. For each AIFS initialization day we test temperature anomaly of the 10 cut-off members with the highest preceding cut-off activity against the entire Z_{500}-matched ensemble mean (c,e), with $p > 0.05$ from one-sided bootstrapping test stippled. (d,f) Vertical temperature anomaly against the Z_{500}-matched ensemble over the UK-France region.

https://doi.org/10.5194/egusphere-2026-6674
Preprint. Discussion started: 13 November 2026
© Author(s) 2026. CC BY 4.0 License.

test whether this observation holds across similar synoptic events, selected from flow analogues of geopotential height across April to August from 1940 to 2025 (Jézéquel et al., 2018).

The seasonal and decadal distribution of the analogues is shown in Figure 4a. We find that no analogue occurs in April, and only two, one cut-off and one no cut-off analogue, before the 25th of May. Instead, the analogues show a clear seasonal signal towards the later summer months. Therefore, we conclude that the occurrence of the circulation pattern in May is highly unusual and even when considering early June such events are highly unlikely. Contrary to previous summer heat extremes with enhanced southerly flow anomalies (Noyelle et al., 2023b; De Vries et al., 2024; Vautard et al., 2023), the May 2026 heatwave shows no clear decadal trend in flow analogues (Fig. 4a).

We then investigate whether the presence of an Iberian cut-off low on the analogue day alters the probability of exceeding a certain temperature threshold, as found for the May 2026 event (Section 3.1). In the cut-off analogue pool, daily mean near surface temperature anomalies over the UK and France increase with preceding cut-off low activity (Figure 4b). Here, preceding cut-off low activity explains 10% of temperature variance ($p = 0.004$), and the relationship strengthens slightly when considering Z_{500}-controlled near surface temperature, i.e. the residual after the linear dependency of MJJA daily mean near surface temperature on Z_{500} is removed. The Z_{500}-controlled relationship is significant at every pool size from $N = 20$ to $N = 85$, although the variance explained beyond Z_{500} decreases from 29 % ($N = 25$) to 13 % ($N = 85$) as analogue quality decreases. Among the 25 to 85 analogues without a cut-off, we find no effect of preceding cut-off low activity on near surface temperature. We conclude that to establish an amplification of near-surface temperature by preceding cut-off low activity, an Iberian cut-off low needs to be present at the analogue date.

The amplification of near surface temperature via cut-off activity further impacts the binary distinction between the cut-off and no cut-off analogues, as found for IFS and AIFS in 3a-b. The cut-off composite has a daily mean surface temperature anomaly shifted positively 0.66 K [0.23, 1.09] of the no cut-off composite (Welch $p = 0.003$; Kolmogorov–Smirnov $p = 0.004$). However, contrary to the IFS and AIFS ensembles for the May 2026 event, this binary distinction is not independent of the UK-France region mean Z_{500}. Cut-off analogues are associated with stronger ridges over the target region and better analogue quality, so that the binary distinction to the no cut-off pool is no longer significant once only the residual, Z_{500}-controlled temperature anomaly is considered (+0.30 K, p = 0.12). In contrast to the IFS/AIFS ensembles, where a shared initial conditions fix the large-scale atmospheric block and the cut-off therefore acts independently of it, in the historical analogues cut-off presence is collinear with the UK-France box Z_{500} and only preceding cut-off low activity adds near surface temperature. Importantly, even when projected to the present day climate, the May 2026 daily mean temperature anomaly sits above all previous analogues, even the 2022 UK heatwave. Thus, the May 2026 heatwave was not only unusual in terms of seasonality but also its daily mean temperature anomaly in comparison with peak summer extremes.

The spatial imprint of strong preceding cut-off low activity within the analogue pool (Fig. 4c) mirrors the results obtained via AIFS for the May 2026 event (Fig. 3c,e). Within the cut-off analogue pool, the composite of the five members with the highest preceding activity shows the most pronounced near-surface temperature amplification over Brittany; The increase is statistically significant across the entire French Atlantic coast and Southern UK. In these regions, the cut-off composite exhibits

https://doi.org/10.5194/egusphere-2026-6674
Preprint. Discussion started: 13 November 2026
© Author(s) 2026. CC BY 4.0 License.

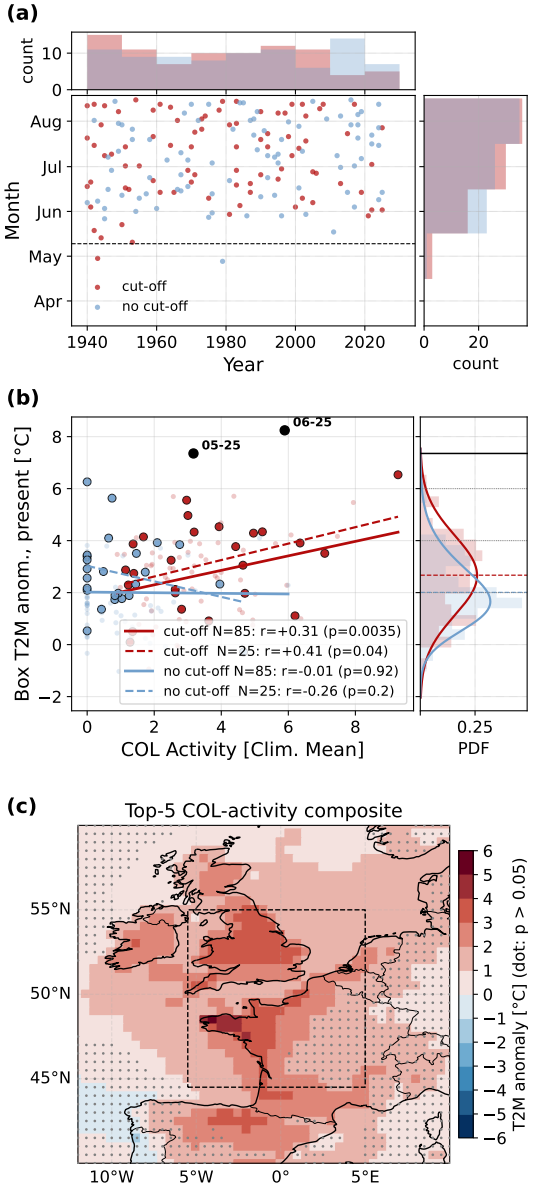


Figure 4. Impact of cut-off low activity across historical analogues. (a) Seasonality and occurrence across decades in the best 85 selected cut-off (red) and no cut-off (blue) analogues between April and August 1940 to 2025 (25th of May as dashed line). (b) To the present day projected temperature anomalies respective to 7 day smoothed 1995 to 2025 climatology across the best 25 (dotted line) and best 85 cut-off (solid line, red) and no cut-off (blue) analogues, against preceding cut-off low activity, with a skew normal distribution fitted to the temperature anomaly distribution (histogram). Included in the analogue selection the June 2026 Heatwave ranks 11th (black). (c) Daily mean surface temperature anomaly of top five cut-off low activity analogues respective to the 85 cut-off and 85 no cut-off pool.

https://doi.org/10.5194/egusphere-2026-6674
Preprint. Discussion started: 13 November 2026
© Author(s) 2026. CC BY 4.0 License.

a daily mean surface temperature anomaly 2°C to 5°C higher than that of the full analogue pool (including both cut-off and no cut-off members).

3.4 Lagrangian analyses of temperature in the UK-France region in ERA5 and IFS

So far we have quantified the effect of an Iberian cut-off low on the May 2026 heatwave and have shown a moderate, but significant increase in near surface temperatures over the UK and France in interaction with the anticyclone due to the cut-off low's presence and preceding activity. As outlined in the introduction, the mechanistic effect of cut-off lows on heatwaves has mostly been implicitly studied, suggesting that Saharan air intrusions and advective warming can co-occur with cut-off low activity (Hotz et al., 2024; Fix et al., 2024; Sousa et al., 2019). Cut-off lows have been statistically associated with western European summer heatwaves (D'Andrea et al., 2024) and appear in simulated and observed record-shattering heatwave dynamics (Noyelle et al., 2023a; Lancelin et al., 2026; Ezber et al., 2026), yet how cut-off lows modify near surface temperatures in such situations remains incompletely understood.

To gain a deeper understanding of the physical mechanisms that drive distinct surface responses to preceding cut-off low activity, we perform a Lagrangian heat decomposition following Röthlisberger and Papritz (2023) on both ERA5 and IFS data (Figure 5). The Lagrangian heat decomposition framework decomposes the total vertical temperature anomaly during the heatwave (Fig. 5a) into contributions via horizontal advection across climatological temperature gradients (advective contributions; Fig. 5b), via vertical motion along anomalous vertical temperature gradients (adiabatic contributions; Fig. 5c) and via changes of potential temperature along the parcel trajectory (diabatic contributions; Fig. 5d). For the May 2026 Heatwave, we find a high dynamical agreement with the July UK 2022 heatwave, as documented by Hotz et al. (2024): the beginning of the heatwave on the 21st of May is driven by a top-down atmospheric control, mainly due to a strong advective influx that reaches throughout the entire atmospheric column. As the atmospheric ridge builds up, adiabatic warming in the mid- to low-troposphere increases. Advective fluxes in the troposphere stay positive throughout the 24th, and carry a positive signal in the lower free troposphere during the heatwave peak throughout the 25th of May. At the near-surface level, strong adiabatic warming builds up throughout the heatwave and is the main process driving near surface temperatures. This adiabatic contribution peaks at heatwave end, and then is offset by an increased diabatic cooling in the lower troposphere, as the air continues to circulate within the heatwave region until the 30th of May (the Lagrangian age at surface level increases without any change of Lagrangian distance; not shown). When restricted to land-only grid points (Supplement Figure S7), diabatic processes in the boundary layer contribute to the surface warming with a clearly visible diurnal cycle.

Atmospheric blocks during heatwaves can be reinforced by upstream latent heating over the North Atlantic (Pfahl et al., 2015; Steinfeld and Pfahl, 2019; Steinfeld et al., 2020). This latent heating predominantly occurs in warm conveyor belt ahead of extratropical cyclones (Madonna et al., 2014; Wernli and Davies, 1997; Heitmann et al., 2024) and can be identified by a rapid increase in potential temperature in upstream air-masses (Zschenderlein et al., 2020; Hotz et al., 2024; Papritz and Röthlisberger, 2023). During the May 2026 heatwave we find that such diabatic processes are of second order compared to advective warming, indicating no strong signal of warm conveyor belts in the heatwave build up between the 21st and 25th.

https://doi.org/10.5194/egusphere-2026-6674
Preprint. Discussion started: 13 November 2026
© Author(s) 2026. CC BY 4.0 License.

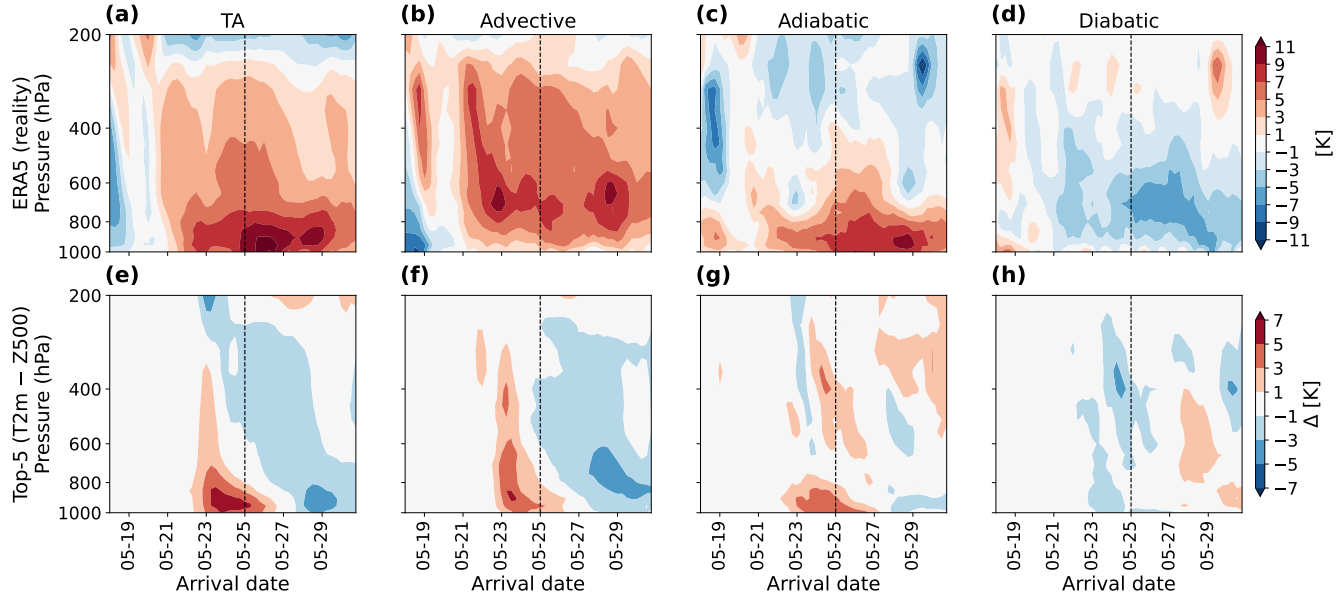


Figure 5. Vertical Lagrangian heat decomposition over the UK-France region for the May 2026 heatwave. The Total temperature anomaly (a,e) is split into Advective (b,f), Adiabatic (c,g) and Diabatic (d,h) contributions. (a-d) Vertical Decomposition in the realized ERA5T event. (e-h) Difference of the temperature anomaly decomposition between the composite of the Top 5 IFS members highest near surface temperature over UK and France minus the top 5 with highest Z_{500} over the same region. The 25th of May 2026 00:00UTC is highlighted as dashed vertical line.

To extract the processes that drive the observed near surface warming difference between the cut-off and no cut-off IFS composites discussed in Figure 1e–f, we continue to perform the Lagrangian heat decomposition framework on the IFS ensemble. Recalling that the top 5 Z_{500} composite in IFS was constructed in exclusion of the top 5 hottest composite (Figure 1e,f), we subtract the first from the second over the vertical decomposition in Figure 5e-h. The top 5 hottest composite shows a distinct warming signal that expands through the entire troposphere on the heatwave beginning (the 23rd of May) and extends through the boundary layer until the 25th of May (Fig. 5e). This temperature anomaly is carried by advective processes in the lower and mid troposphere from the 23rd until the 25th of May (Fig. 5f). Near surface warming is further enhanced by increased adiabaticity in the boundary layer (Fig. 5g). Diabatic processes play a minor role in the boundary layer (Fig. 5h), even when land-only grid points are considered (Supplement Figure S7.) In the IFS ensemble the hottest 5 members have a shorter persistence compared to the top 5 Z_{500} composite, leading to slightly higher near surface temperature anomalies in the Z_{500} composite during the heatwave decay. The bias of the hottest 5 member composites with ERA5 (Supplement Figure S6), shows that the heatwave persistence is underestimated by this IFS composite due to a stronger atmospheric anticyclone in ERA5 (higher Z_{500} over the target region) which translates to increased adiabatic heating. In contrast, the top 5 Z_{500} IFS members underestimate near surface temperature at the heatwave peak on the 25th of May because the composite misses the exact

https://doi.org/10.5194/egusphere-2026-6674
Preprint. Discussion started: 13 November 2026
© Author(s) 2026. CC BY 4.0 License.

same signature that is conveyed by the hottest 5 IFS members in Figure 5f and 5g: an enhanced advective process throughout the atmospheric column on the 23rd and enhanced adiabatic warming on the heatwave peak.

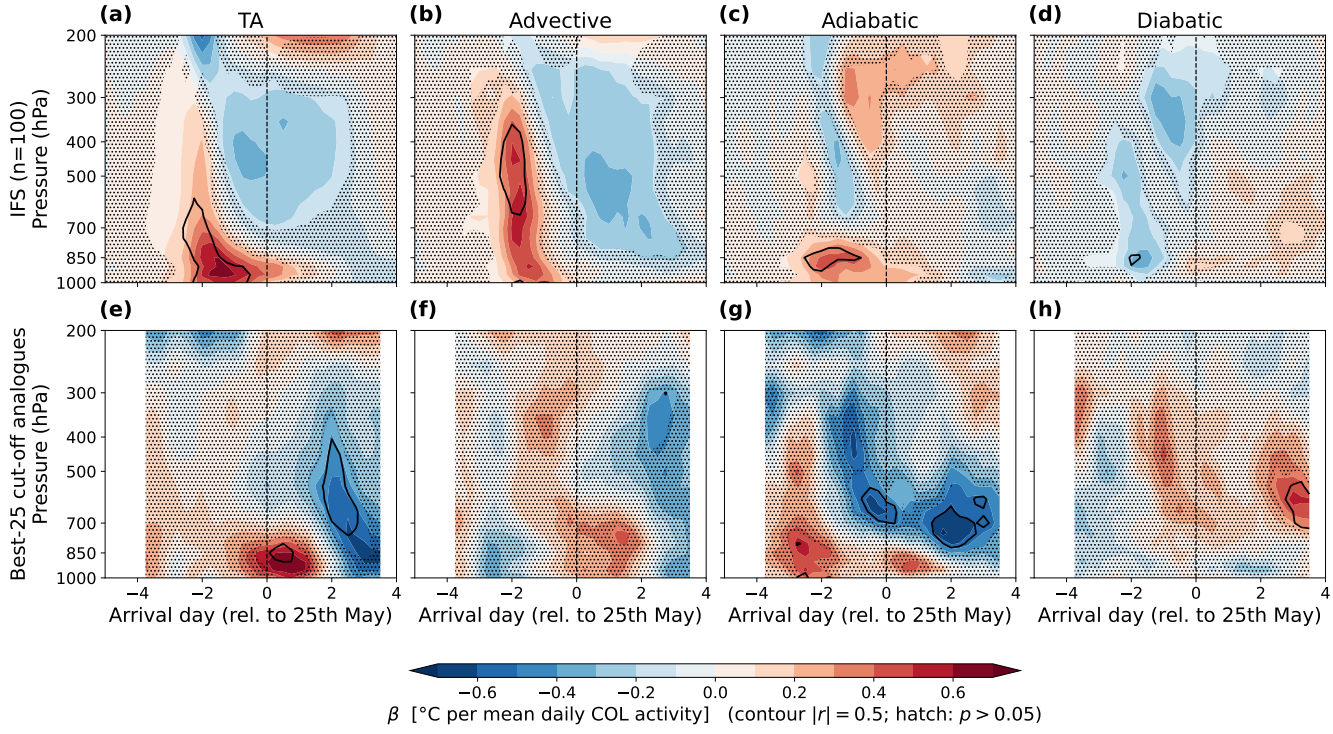


Figure 6. Regression of preceding cut-off low activity against vertical Lagrangian heat decomposition over the UK-France Region Processes for each row as in Figure 5. (a-d) OLS slope of cut-off low activity against temperature anomaly decomposition across IFS members (init 17th and 18th of May) (e-h) OLS slopes across the best 25 respective cut-off analogue dates. Nonsignificant slopes, following a Pearson test, are shaded. Altitudes of Pearson correlation higher than 0.5 in black contours. The 25th of May 2026 00:00UTC is highlighted as dashed vertical line.

Noting that Figure 5e yields consistency with the AIFS-ENS sensitivity analysis above (Figure 3d–f), we verify that the difference between the two IFS composites is representative of enhanced preceding cut-off low activity. We do so by linearly regressing preceding cut-off low activity on the vertical profile of each process (Figure 6). Linear regression slopes are computed for both IFS and the best 25 cut-off analogues. Consistent with the difference between the IFS composites, preceding Cut-off activity enhances a deep, mid-tropospheric advective branch arriving two day prior to the 25th together with an enhanced adiabatic warming during the heatwave peak. The low tropospheric adiabatic warming, conveying heat to the boundary layer, results from an enhanced subsidence velocity and dominating compression term rather than changes in the climatological temperature gradient (see both terms in equation 5). We tentatively interpret this result as a subsequent coupling of the mid tropospheric branch to the near surface layer. We cannot rule out a contribution from entrainment of warmer air at the boundary-layer top, but our Lagrangian setup does not properly resolve turbulent entrainment, and the subsidence maximum just above

https://doi.org/10.5194/egusphere-2026-6674
Preprint. Discussion started: 13 November 2026
© Author(s) 2026. CC BY 4.0 License.

the boundary layer may partly reflect this limitation. The analogues reproduce the adiabatic warming around 850 hPa, but not the mid-tropospheric advective signal to a significant extent. The link between cut-off activity, the advective branch, and near-surface temperatures will be further discussed in the next section. Prior to the heatwave peak, the diabatic signal in the analogues carries the opposite sign of IFS, though the contribution is non-significant in the analogues. We hypothesize that this is because some of the analogues show a stronger warm conveyor belt signal over the western North Atlantic than the May 2026 heatwave (Supplement Figure S9d).

From Figures 5 and 6, we learn that in the mid-troposphere, preceding cut-off low activity alters the advective transport prior to the heatwave peak. The mid tropospheric branch preconditions the surface response, as this surplus is gradually transferred to the boundary layer via enhanced subsidence. In the heat decomposition framework, such advective processes are derived from climatological, horizontal temperature gradients. As such they are associated with specific atmospheric pathways. In particular Saharan air intrusion has been reported to co-occur with cut-off low activity during previous heatwaves in previous tracer analyses (Fix et al., 2024; Fix-Hewitt et al., 2026; Vautard et al., 2020). In the following section, we will therefore test the impact of cut-off low activity on the movement of air masses by introducing a novel trajectory origin contribution analysis which we couple to the temperature decomposition above.

3.5 Iberian cut-off lows enhance heat transport from Sahara

Now we test the hypothesis that these advective processes are driven by the presence of the cut-off low. As advective warming in the heat decomposition framework is defined as trajectory movement across horizontal temperature gradients (Röthlisberger and Papritz, 2023), the origin and horizontal pathway of a parcel mainly influence the final outcome of this variable. To test for statistical links between the origin of the process contribution, preceding cut-off low activity and near surface temperature, we generate the origin contribution map described in the methods section for every IFS member. We later evaluate the linear regression slopes between the ensemble maps with preceding Iberian cut-off activity and the linear regression slopes between the ensemble maps with daily mean surface temperature over the UK France box on the 25th of May.

We find that from the 24th to the 25th of May at 850 to 1000 hPa arrival level, where the advective heat difference between the two IFS composites in Figure 5 is strongest, the main difference in the origin of advective heat sits over the Western Sahara and Morocco (Supplement Figure S8a). Here, the integrated contribution difference between 20°W–0° longitude and 25°N–40°N latitude is about 0.88°C across both days. Consistent with the previous section, we find that the amplification of the Saharan branch is strongly represented in the mid tropospheric arrival band between 250 to 750 hPa (Figure S8b). The mid-tropospheric branch is our preferable choice for further analysis compared to the near surface level, as it directly connects to the cut-off low analysis centered around 500 hPa.

Aggregated over all trajectories arriving between 250 hPa and 750h Pa over the 24th to the 25th of May we obtain Figure 7a for the positive advective branch of ERA5 (Supplement Figure S10 shows all process maps). The ERA5 origin contribution map shows a strong advective branch originating over the Saharan coast, extending over the Canary Islands up to the Iberian Peninsula. Further branching occurs from the West tropical North Atlantic, Mexico and the US. The dominant North American branch is well reproduced by the IFS model. The Saharan branch is much stronger in the realized ERA5 event than in the

https://doi.org/10.5194/egusphere-2026-6674
Preprint. Discussion started: 13 November 2026
© Author(s) 2026. CC BY 4.0 License.

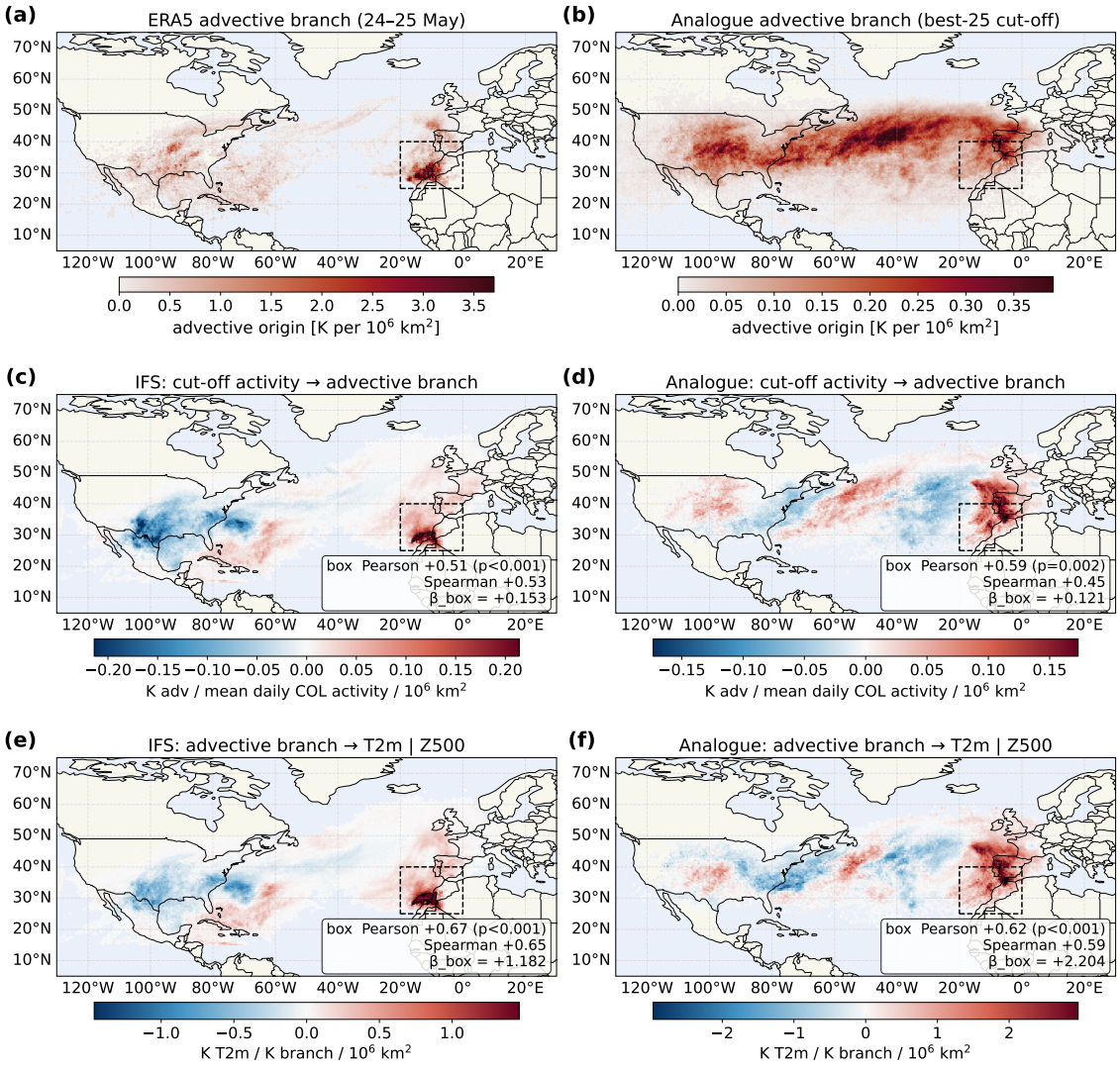


Figure 7. Genesis locations of 250-750 hPa advective temperature anomaly contributions to the UK-France region and their regression slopes with preceding cut-off low activity and near surface temperatures. Advective origin contribution map aggregated over the 24th to the 25th of May for ERA5 (a) and for the best 25 analogues (b), positive grid cells only. (c) Regression slope of advective origin contributions across IFS Members from Initializations of 17th and 18th of May with persistent cut-off low activity preceding the 25th of May and (e) with daily mean surface temperature at the 25th of May. Panel (d) same as (c) across the best 25 cut-off analogues using the respective analogue date instead of the 25th of May as reference. Panel (f) as (e) for the same analogues. Box integrated linear regression slopes β, as referred to in the legend, are not normalized by area.

IFS ensemble mean, but also the west tropical North Atlantic branch is slightly underrepresented, meaning the forecast underrepresents the advective import from these regions. This is consistent with the exceptional strength of the realized Saharan

https://doi.org/10.5194/egusphere-2026-6674
Preprint. Discussion started: 13 November 2026
© Author(s) 2026. CC BY 4.0 License.

branch and, as we will now see, with a higher near surface response of ERA5 compared to IFS. We use the IFS pool to extract the origin regions which drive enhanced advective warming observed in the previous section (Figure 7c,e). A linear regression between preceding cut-off low activity and the advective contribution of each cell (Figure 7c) highlights regions which have the strongest link to preceding cut-off low activity within the IFS ensemble. While the US-Mexican branch shows significant negative dependence of branch activity on preceding cut-off low activity, the Saharan branch shows the strongest positive dependency. The average over the entire Saharan box shows that preceding cut-off low activity explains more than 25% of the branch variance. The effect of the advective branch on the near-surface temperature reveals the same spatial pattern and similarly strong statistical link of the Saharan branch on the near surface temperature over the UK and France.

We again cross-validate the IFS results on the pooled best 25 cut-off analogues. The analogue pool's upper tropospheric pathways agree with known upper tropospheric Lagrangian dynamics of summer heatwaves (Zschenderlein et al., 2020) (Figure 7b): The origin contribution analysis reveals a (remote) strong advective branch along the US and across the West Subtropical North Atlantic into the Heatwave region. Distinct from this branch is a second (nearby) pathway from the Saharan region through the Iberian Peninsula. Importantly, both of these branches carry different diabatic signals consistent with Zschenderlein et al. (2020). The remote branch is intensified through diabatic heating, whereas the nearby branch is diabatically cooled (Supplement Figure S9).

The analogue results are dynamically consistent with the IFS results, with strong statistical links to advective origin over the Iberian Peninsula, Gibraltar and Morocco. For the Box integrated values we find agreement between the analogue pool with what is observed in IFS. Here, persistent cut-off low activity amplifies the nearby advective branch, explaining about 35% of the branch's variance (Fig 7d). In turn, the nearby branch explains 38% of the UK–France near surface temperature variance (Fig. 7f). Comparing the analogue analysis with the IFS shows that the nearby branch is the only consistent pathway that survives this cross validation. We hence show that preceding cut-off low activity not merely enhances advective warming per se, but particularly strengthens the movement of air masses from nearby branches most strongly linked to increases in near surface temperatures. In case of May 2026, the genesis of temperature anomalies happened unprecedentedly far South within the nearby branch compared to the analogue pool (Figure 7a vs 7b), providing a possible explanation for the large margin by which UK-France near surface temperature anomalies in May 2026 differed to similar past synoptic events (Figure 4b).

4 Discussion

The atmospheric pattern of the May 2026 heatwave is frequently associated with late summer heatwaves in the ERA5 reanalysis, but rarely found in early season heatwaves such as May and June. Importantly, we find high synoptic and dynamical agreement between the May 2026 and the June 2026 Heatwave, as well as between the May 2026 Heatwave and the July 2022 Heatwave; both of these events rank in the top 25 cut-off analogues if 2026 is included in the analysis (Figure 4b). Both heatwaves yielded record-breaking temperatures over the Southern UK and the French Atlantic coast. We therefore repeat the analysis of Figure 4b for the July 2022 and June 2026 heatwave dates, as they both represent record-shattering events synoptically similar to the May 2026 event (Supplement Figure S11). The statistical link at $N = 85$ between preceding cut-off low

https://doi.org/10.5194/egusphere-2026-6674
Preprint. Discussion started: 13 November 2026
© Author(s) 2026. CC BY 4.0 License.

activity and daily mean near surface temperature appears similar or stronger in these examples ($r = 0.33$ for July 2022 and $r = 0.40$ for June 2026; robust to Z_{500}-control, not shown). Hence, the findings of this paper hold importance to understand recent record-shattering, cut-off low amplified heatwaves beyond the specific case of May 2026.

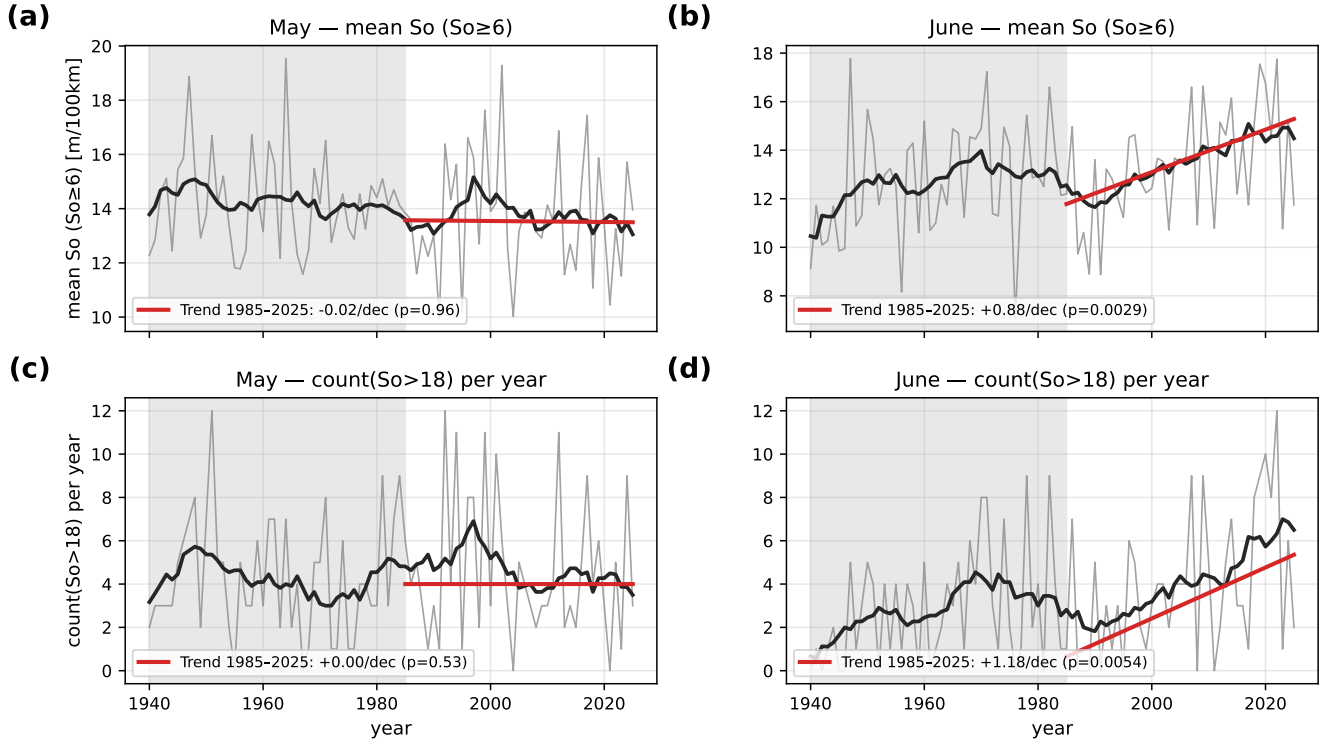


Figure 8. Seasonal changes in Iberian cut-off low intensity and frequency between 1940 and 2025 (a) May mean Iberian cut-off intensity, measured as optimal slope So on 500 hPa geopotential height contours, (b) for the month of June. (c) Intense cut-off low occurrence (number of days with optimal slope $So > 18$ m per 100 km) for the month of May, (d) for the month of June. The 11-year-running means is shown in black and linear 1985 to 2025 trend in red.

The extreme early season heat of 2026 raises the question of how such rare events can appear twice sequentially within the time span of 30 days. In contrast to previous studies on Southerly Flow anomalies in spring (Noest et al., 2026), we do not find evidence for significant dynamical trends in neither May nor June analogues. However, we do find a significant increase of Iberian cut-off low activity for the month of June (Figure 8b). The trend is mainly driven by an increased occurrence of intense Iberian cut-off lows (So > 18 m (100 km)$^{-1}$), rising with a trend of 1.18 days per decade since 1985 (Figure 8d). The finding of more intense Iberian cut-off lows is in agreement with previous studies on summer North Atlantic deep depressions (D'Andrea et al., 2024), and requires an in depth investigation of whether this signal is anthropogenically forced or not, which is beyond the scope of this study.

https://doi.org/10.5194/egusphere-2026-6674
Preprint. Discussion started: 13 November 2026
© Author(s) 2026. CC BY 4.0 License.

5 Conclusions

This paper puts together an ensemble of methods (Lagrangian analysis, analogues of circulation) and datasets (reanalysis, ensemble forecasts) to provide a thorough climatological and meteorological analysis of the exceptional May 2026 heat event that struck France and Southern UK.

We showed that:

- the primary source of heat came from record-breaking anticyclonic conditions over France (the so-called Omega block). This pattern alone contributed to half of the temperature anomaly ($+ \approx 2.8$°C) over France and Southern UK through adiabatic heating, but does not explain the entirety of the observed temperature anomaly ($+ \approx 7.4$°C).
- a cut-off low over the Iberian Peninsula dynamically amplified the heatwave to a record-breaking extent in interaction with an unprecedentedly strong ridge. Using large ensemble medium range forecasts (IFS and AIFS) we quantified the effect of the Iberian cut-off low and showed that its impact is localized, mainly amplifying temperatures near the French Atlantic coast and southern UK by up to 4.5°C.
- preceding cut-off low activity amplifies advective heating in the mid troposphere and increases subsidence near the boundary layer top. This was found by applying a Lagrangian temperature anomaly decomposition to the 100 members of the perturbed IFS forecast and 25 synoptic circulation analogues.
- by linking the mid-tropospheric advective contribution to its genesis location, the amplification of near surface temperatures via preceding cut-off low activity can be explained by the amplification of a nearby Saharan Branch,
- compared to other, synoptically similar events, the Saharan branch in May 2026 emerged unprecedentedly far south. The contribution of the branch was underestimated in the IFS forecast initialized 7 and 8 days before heatwave peak.
- the diabatic term (due to latent heat fluxes) cooled the lower troposphere, suggesting that temperatures could have been higher if the beginning of May had not been wet in Western Europe.
- the circulation pattern of the May 2026 heatwave is typically associated with late summer month, and its occurrence in May, even in the beginning of June is highly unusual. The closest May analogue is found for the May 1944 heatwave (Holliday et al., 2026), i.e. appears in the first decade of the ERA5 record.

During the May 2026 heatwave preceding cut-off low activity was neither remarkable in its intensity nor persistence, yet amplified near-surface heat by establishing a mid-tropospheric branch deep into the coastal North-western African region over Morocco and West Sahara prior to the heatwave peak. The established airflow then amplified near surface heat (due to anticyclonic conditions over France), as the cut-off low enhanced subsidence near the boundary layer in the following days. The impact was highly localized in the downstream interface between the ridge and the cut-off low, namely over Northern Spain, the French Atlantic Coast and Southern UK, exactly where record-breaking temperatures occurred. We find that the dynamic

https://doi.org/10.5194/egusphere-2026-6674
Preprint. Discussion started: 13 November 2026
© Author(s) 2026. CC BY 4.0 License.

of cut-off low amplified near surface temperatures likely played a role during record-shattering extremes in the Southern-UK Western France region with similar atmospheric patterns, such as during the July 2022 and the June 2026 heatwave.

Although this paper is not an extreme event attribution study (National Academies of Sciences Engineering and Medicine, 2016), we argue that the approach that we followed could complement analyses of extreme events that are based on the atmospheric circulation (Faranda et al., 2024). This could be done by analyzing the terms of the temperature decomposition (rather than just their sum at the surface), and by focusing the search of analogues on the separate occurrence of cut-off lows and anticyclonic conditions (e.g., with methods developed by Fery et al. (2022), possibly extending the analogue search to the CMIP model world (Riboldi et al., 2026)). This is close to a *storyline* approach (Shepherd, 2019) of attribution, by identifying the physical mechanisms leading to extreme heat. The analysis of analogues shows that the occurrence of intense Iberian cut-off during June has significantly increased since 1985, whether anthropogenically forced or no, remains open for further investigation. As the near-surface impact increases with preceding Iberian cut-off low intensity, an increase in such activity can have highly localized impact on France and the UK, especially when coupled to the formation of strong ridges. This analysis is coherent with the increasing duration of the warm season in Europe (Peña-Ortiz et al., 2015).

Overall, this analysis was able to relate large-scale atmospheric structures to the temperature evolution processes over the atmospheric column. This exercise is necessary to understand and anticipate the (future) evolution of the most extreme heat events, beyond statistical analyses of surface temperature time series.

Code and data availability. Analysis scripts are available on github (https://github.com/maevemayer/may2026-heatwave) and the derived data on Zenodo (10.5281/zenodo.23666703). IFS ensemble forecasts for geopotential height on pressure levels and near surface temperature can be downloaded from the TIGGE Archive (ECMWF Data Store Service, 2026; Bougeault et al., 2010; ECMWF, 2026). ERA5 reanalysis data can be downloaded from the Copernicus Climate Data Store (Soci et al., 2024). The AIFS-Ens v1 model with weights is available on HuggingFace (https://huggingface.co/ecmwf/aifs-ens-1.0, last accessed : 26/10/2026)

https://doi.org/10.5194/egusphere-2026-6674
Preprint. Discussion started: 13 November 2026
© Author(s) 2026. CC BY 4.0 License.

Author contributions. Maeve Mayer conceived and coordinated the study, designed the methodology, implemented the cut-off detection on IFS forecasts and past ERA5 events, performed the Lagrangian decomposition of analogues, and drafted the original version of the manuscript together with Pascal Yiou and Paolo Chevalier. Paolo Chevalier and Belinda Hotz contributed equally and substantially to the results. Paolo Chevalier performed the AIFS simulations and sensitivity analyses. Belinda Hotz performed the Lagrangian analyses on the IFS forecasts. Pascal Yiou, Soulivanh Thao and Robin Noyelle supervised the study. Belinda Hotz, Soulivanh Thao and Robin Noyelle further contributed to the writing of the manuscript. Claire Petter reviewed the manuscript and supervises the PhD thesis of Maeve Mayer.

Competing interests. The authors declare that they have no conflict of interest.

Acknowledgements. We gratefully thank Dr. Leonard Borchert for providing the resources to run the Lagrangian decomposition for the ERA5 flow analogues on the German Climate Computing Center DKRZ. Further, it has been a pleasure to exchange with Satoru Kasuga on this project and we would like to thank him for providing the cut-off low identification tool colindex2 publicly, well-documented and easily accessible. We are grateful to MeteoSwiss and ECMWF for granting access to the operational IFS forecasts. We would like to thank Daniela Domeisen for sparking the idea of using perturbed ensemble IFS archive data. It is a pleasure to thank Jeanne Vedel who installed a first version of AIFS on Jean-Zay. We acknowledge discussions with Sylvie Parey and Thibault Lemaître-Basset, who participated to Maeve Mayer's PhD supervision. This project was provided with HPC resources by GENCI at IDRIS thanks to the grant 2026-AD010116371R1 on the supercomputer Jean Zay's A100 partition. The authors used Claude Code to assist with revising and generating Python plotting and analysis scripts and checking the manuscript for numerical consistency. All code, results and text were reviewed and verified by the authors, who take full responsibility for the content of this article.

Financial support. Belinda Hotz and Robin Noyelle have received funding from the Schweizerischer Nationalfonds zur Förderung der Wissenschaftlichen Forschung (grant nos. 219244 and 216710, respectively). This study has further received funding from the Agence Nationale de la Recherche – France 2030 as part of the PEPR TRACCS programme (grant no. ANR-22-EXTR-0005) and from the Horizon Europe project CLOSER (grant no. 101293581).

https://doi.org/10.5194/egusphere-2026-6674
Preprint. Discussion started: 13 November 2026
© Author(s) 2026. CC BY 4.0 License.

References

Barriopedro, D., García-Herrera, R., Ordóñez, C., Miralles, D. G., and Salcedo-Sanz, S.: Heat Waves: Physical Understanding and Scientific Challenges, Reviews of Geophysics, 61, e2022RG000 780, https://doi.org/10.1029/2022RG000780, 2023.

Bougeault, P., Toth, Z., Bishop, C., Brown, B., Burridge, D., Chen, D. H., Ebert, B., Fuentes, M., Hamill, T. M., Mylne, K., Nicolau, J., Paccagnella, T., Park, Y.-Y., Parsons, D., Raoult, B., Schuster, D., Dias, P. S., Swinbank, R., Takeuchi, Y., Tennant, W., Wilson, L., and Worley, S.: The THORPEX Interactive Grand Global Ensemble, Bulletin of the American Meteorological Society, 91, 1059–1072, https://doi.org/10.1175/2010BAMS2853.1, 2010.

Copernicus Climate Change Service: Complete ERA5 global atmospheric reanalysis, https://doi.org/10.24381/CDS.143582CF, 2023.

D'Andrea, F., Duvel, J.-P., Rivière, G., Vautard, R., Cassou, C., Cattiaux, J., Coumou, D., Faranda, D., Happé, T., Jézéquel, A., Ribes, A., and Yiou, P.: Summer Deep Depressions Increase Over the Eastern North Atlantic, Geophysical Research Letters, 51, e2023GL104 435, https://doi.org/10.1029/2023GL104435, 2024.

De Vries, H., Lenderink, G., Van Meijgaard, E., Van Ulft, B., and De Rooy, W.: Western Europe's extreme July 2019 heatwave in a warmer world, Environmental Research: Climate, 3, 035 005, https://doi.org/10.1088/2752-5295/ad519f, 2024.

Domeisen, D. I. V., Eltahir, E. A. B., Fischer, E. M., Knutti, R., Perkins-Kirkpatrick, S. E., Schär, C., Seneviratne, S. I., Weisheimer, A., and Wernli, H.: Prediction and projection of heatwaves, Nature Reviews Earth & Environment, 4, 36–50, https://doi.org/10.1038/s43017-022-00371-z, 2022.

Ebi, K. L., Capon, A., Berry, P., Broderick, C., De Dear, R., Havenith, G., Honda, Y., Kovats, R. S., Ma, W., Malik, A., Morris, N. B., Nybo, L., Seneviratne, S. I., Vanos, J., and Jay, O.: Hot weather and heat extremes: health risks, The Lancet, 398, 698–708, https://doi.org/10.1016/S0140-6736(21)01208-3, 2021.

ECMWF: IFS Documentation CY50R1 - Part 5: Ensemble Prediction System, https://doi.org/10.21957/04568076AC, 2026.

ECMWF Data Store Service: TIGGE global medium-range ensemble forecasts from multiple NWP centres since 2006, https://doi.org/10.21957/8511726F, 2026.

Ezber, Y., Toker, E., Barnes, M. A., Reboita, M., and Chun, K. P.: Dynamic drivers of an extreme heatwave over the UK in July 2022, Scientific Reports, https://doi.org/10.1038/s41598-026-65523-3, 2026.

Faranda, D., Messori, G., Coppola, E., Alberti, T., Vrac, M., Pons, F., Yiou, P., Saint Lu, M., Hisi, A. N. S., Brockmann, P., Dafis, S., Mengaldo, G., and Vautard, R.: ClimaMeter: contextualizing extreme weather in a changing climate, Weather Clim. Dynam., 5, 959–983, https://doi.org/10.5194/wcd-5-959-2024, 2024.

Fery, L., Dubrulle, B., Podvin, B., Pons, F., and Faranda, D.: Learning a Weather Dictionary of Atmospheric Patterns Using Latent Dirichlet Allocation, Geophysical Research Letters, 49, e2021GL096 184, https://doi.org/10.1029/2021GL096184, 2022.

Fix, F., Mayr, G., Zeileis, A., Stucke, I., and Stauffer, R.: Detection and consequences of atmospheric deserts: insights from a case study, Weather and Climate Dynamics, 5, 1545–1560, https://doi.org/10.5194/wcd-5-1545-2024, 2024.

Fix-Hewitt, F., Zeileis, A., Stucke, I., Stauffer, R., and Mayr, G. J.: Properties and characteristics of atmospheric deserts over Europe: a first statistical analysis, Weather and Climate Dynamics, 7, 17–35, https://doi.org/10.5194/wcd-7-17-2026, 2026.

Gasparrini, A., Guo, Y., Hashizume, M., Lavigne, E., Zanobetti, A., Schwartz, J., Tobias, A., Tong, S., Rocklöv, J., Forsberg, B., Leone, M., De Sario, M., Bell, M. L., Guo, Y.-L. L., Wu, C.-f., Kan, H., Yi, S.-M., de Sousa Zanotti Stagliorio Coelho, M., Saldiva, P. H. N., Honda, Y., Kim, H., and Armstrong, B.: Mortality risk attributable to high and low ambient temperature: a multicountry observational study, The Lancet, 386, 369–375, https://doi.org/10.1016/S0140-6736(14)62114-0, 2015.

https://doi.org/10.5194/egusphere-2026-6674
Preprint. Discussion started: 13 November 2026
© Author(s) 2026. CC BY 4.0 License.

González-Alemán, J. J., Oltmanns, M., Gonzalez-Herrero, S., Donat, M., Vitart, F., Doblas Reyes, F., Barriopedro, D., Riboldi, J., Calvo-Sancho, C., Jiménez-Esteve, B., Cos, P., and Wehner, M.: Emerging links between Greenland ice melt, Euro-Mediterranean heat extremes, and destructive convective storms, https://doi.org/10.31223/X5QR3N, 2026.

Heitmann, K., Sprenger, M., Binder, H., Wernli, H., and Joos, H.: Warm conveyor belt characteristics and impacts along the life cycle of extratropical cyclones: case studies and climatological analysis based on ERA5, Weather and Climate Dynamics, 5, 537–557, https://doi.org/10.5194/wcd-5-537-2024, 2024.

Holliday, R., McCarthy, M., Pirret, J., and Wallace, E.: Record-breaking May heat in the UK : contrasting the extreme temperatures of 2024 and 1944 using climate attribution, Weather, 81, 146–153, https://doi.org/10.1002/wea.7740, 2026.

Hotz, B., Papritz, L., and Röthlisberger, M.: Understanding the vertical temperature structure of recent record-shattering heatwaves, Weather and Climate Dynamics, 5, 323–343, https://doi.org/10.5194/wcd-5-323-2024, 2024.

Ionita, M. and Nagavciuc, V.: The June 2026 heatwave established a new benchmark for early-summer heat in German, https://doi.org/10.5194/egusphere-2026-4179, 2026.

Ivanovich, C. C., Cook, B., and McDermid, S.: Extreme Dry and Humid Heat Seasons Are Changing Asymmetrically, AGU Advances, 7, e2026AV002 516, https://doi.org/10.1029/2026AV002516, 2026.

Jézéquel, A., Yiou, P., and Radanovics, S.: Role of circulation in European heatwaves using flow analogues, Climate Dynamics, 50, 1145–1159, https://doi.org/10.1007/s00382-017-3667-0, 2018.

Kasuga, S.: colindex2: A Python Package for Detection and Tracking, https://gitlab.com/kasugab3621/colindex2, accessed: 2026-08-25, 2022.

Kasuga, S., Honda, M., Ukita, J., Yamane, S., Kawase, H., and Yamazaki, A.: Seamless Detection of Cutoff Lows and Preexisting Troughs, Monthly Weather Review, https://doi.org/10.1175/MWR-D-20-0255.1, 2021.

Kovats, R. S. and Kristie, L. E.: Heatwaves and public health in Europe, European Journal of Public Health, 16, 592–599, https://doi.org/10.1093/eurpub/ckl049, 2006.

Lancelin, A., Wikner, A., Dubus, L., Le Priol, C., Abbot, D. S., Bouchet, F., Hassanzadeh, P., and Weare, J.: AI-Boosted Rare Event Sampling to Characterize Extreme Weather, Physical Review Letters, 137, 064 201, https://doi.org/10.1103/b1gc-9c2q, 2026.

Lang, S., Alexe, M., Clare, M. C. A., Roberts, C., Adewoyin, R., Ben Bouallègue, Z., Chantry, M., Dramsch, J., Dueben, P. D., Hahner, S., Maciel, P., Prieto-Nemesio, A., O'Brien, C., Pinault, F., Polster, J., Raoult, B., Tietsche, S., and Leutbecher, M.: AIFS-CRPS: ensemble forecasting using a model trained with a loss function based on the continuous ranked probability score, npj Artificial Intelligence, 2, 18, https://doi.org/10.1038/s44387-026-00073-7, 2026.

Madonna, E., Wernli, H., Joos, H., and Martius, O.: Warm Conveyor Belts in the ERA-Interim Dataset (1979–2010). Part I: Climatology and Potential Vorticity Evolution, Journal of Climate, 27, 3–26, https://doi.org/10.1175/JCLI-D-12-00720.1, 2014.

Mishra, A. N., Maraun, D., Schiemann, R., Hodges, K., Zappa, G., and Ossó, A.: Long-lasting intense cut-off lows to become more frequent in the Northern Hemisphere, Communications Earth & Environment, 6, 115, https://doi.org/10.1038/s43247-025-02078-7, 2025.

Mittermeier, M., Grams, C. M., Beyerle, U., Suarez-Gutierrez, L., Bevacqua, E., Guo, Y., Zscheischler, J., and Fischer, E. M.: Omega-blocks with spatially compounding extremes over Europe are highly sensitive to remote atmospheric drivers, https://doi.org/10.48550/ARXIV.2603.27392, version Number: 1, 2026.

Muñoz, C., Schultz, D., and Vaughan, G.: A Midlatitude Climatology and Interannual Variability of 200- and 500-hPa Cut-Off Lows, Journal of Climate, 33, 2201–2222, https://doi.org/10.1175/JCLI-D-19-0497.1, 2020.

https://doi.org/10.5194/egusphere-2026-6674
Preprint. Discussion started: 13 November 2026
© Author(s) 2026. CC BY 4.0 License.

Météo France: Pourquoi l'épisode de chaleur de fin mai est-il inédit par sa précocité?, https://meteofrance.com/actualites/pourquoi-lepisode-de-chaleur-de-fin-mai-est-il-inedit-par-sa-precocite, last access: 13 October 2026, 2026a.

Météo France: Bilan climatique de l'été 2026 (juin-juillet-août), https://meteofrance.com/presse/bilan-climatique-de-lete-2026-juin-juillet-aout, last access: 13 October 2026, 2026b.

National Academies of Sciences Engineering and Medicine, ed.: Attribution of Extreme Weather Events in the Context of Climate Change, The National Academies Press, Washington, DC, https://doi.org/10.17226/21852, 2016.

Nieto, R., Gimeno, L., De La Torre, L., Ribera, P., Gallego, D., García-Herrera, R., García, J. A., Nuñez, M., Redaño, A., and Lorente, J.: Climatological Features of Cutoff Low Systems in the Northern Hemisphere, Journal of Climate, 18, 3085–3103, https://doi.org/10.1175/JCLI3386.1, 2005.

Noest, D. S., Pinto, I., Thompson, V., and Coumou, D.: The role of atmospheric circulation changes in Western European warm season heat extremes, Weather and Climate Dynamics, 7, 439–452, https://doi.org/10.5194/wcd-7-439-2026, 2026.

Noyelle, R., Yiou, P., and Faranda, D.: Investigating the typicality of the dynamics leading to extreme temperatures in the IPSL-CM6A-LR model, Climate Dynamics, https://doi.org/10.1007/s00382-023-06967-5, 2023a.

Noyelle, R., Zhang, Y., Yiou, P., and Faranda, D.: Maximal reachable temperatures for Western Europe in current climate, Environmental Research Letters, 18, 094 061, https://doi.org/10.1088/1748-9326/acf679, 2023b.

Noyelle, R., Faranda, D., Robin, Y., Vrac, M., and Yiou, P.: Attributing the occurrence and intensity of extreme events with the flow analogue method, Weather Clim. Dynam., 6, 817–839, https://doi.org/10.5194/wcd-6-817-2025, 2025.

Pappert, D., Tuel, A., Coumou, D., Vrac, M., and Martius, O.: Long vs. short: understanding the dynamics of persistent summer hot spells in Europe, Weather and Climate Dynamics, 6, 769–788, https://doi.org/10.5194/wcd-6-769-2025, 2025.

Papritz, L. and Röthlisberger, M.: A Novel Temperature Anomaly Source Diagnostic: Method and Application to the 2021 Heatwave in the Pacific Northwest, Geophysical Research Letters, 50, e2023GL105 641, https://doi.org/10.1029/2023GL105641, 2023.

Peña-Ortiz, C., Barriopedro, D., and García-Herrera, R.: Multidecadal Variability of the Summer Length in Europe, Journal of Climate, 28, 5375 – 5388, https://doi.org/10.1175/JCLI-D-14-00429.1, 2015.

Pfahl, S. and Wernli, H.: Quantifying the relevance of atmospheric blocking for co-located temperature extremes in the Northern Hemisphere on (sub-)daily time scales, Geophysical Research Letters, 39, 2012GL052 261, https://doi.org/10.1029/2012GL052261, 2012.

Pfahl, S., Schwierz, C., Croci-Maspoli, M., Grams, C. M., and Wernli, H.: Importance of latent heat release in ascending air streams for atmospheric blocking, Nature Geoscience, 8, 610–614, https://doi.org/10.1038/ngeo2487, 2015.

Portmann, R., Sprenger, M., and Wernli, H.: The three-dimensional life cycles of potential vorticity cutoffs: a global and selected regional climatologies in ERA-Interim (1979–2018), Weather and Climate Dynamics, 2, 507–534, https://doi.org/10.5194/wcd-2-507-2021, 2021.

Riboldi, J., Noyelle, R., Agayar, E., Binder, H., Federer, M., Hartmuth, K., Sprenger, M., Thurnherr, I., and Vishnupriya, S.: Storm Boris (2024) in the current and future climate: a dynamics-centered contextualization, and some lessons learnt, Weather and Climate Dynamics, 7, 65–87, https://doi.org/10.5194/wcd-7-65-2026, 2026.

Röthlisberger, M. and Papritz, L.: Quantifying the physical processes leading to atmospheric hot extremes at a global scale, Nature Geoscience, 16, 210–216, https://doi.org/10.1038/s41561-023-01126-1, 2023.

Scott, T. J., White, R. H., and Donner, S. D.: Summers over land and ocean are becoming longer, transitioning faster, and accumulating more heat, Environmental Research Letters, 21, 074 009, https://doi.org/10.1088/1748-9326/ae5724, 2026.

Shepherd, T. G.: Storyline approach to the construction of regional climate change information, Proceedings of the Royal Society A: Mathematical, Physical and Engineering Sciences, 475, 20190 013, https://doi.org/10.1098/rspa.2019.0013, 2019.

https://doi.org/10.5194/egusphere-2026-6674
Preprint. Discussion started: 13 November 2026
© Author(s) 2026. CC BY 4.0 License.

Soci, C., Hersbach, H., Simmons, A., Poli, P., Bell, B., Berrisford, P., Horányi, A., Muñoz-Sabater, J., Nicolas, J., Radu, R., Schepers, D., Villaume, S., Haimberger, L., Woollen, J., Buontempo, C., and Thépaut, J.: The ERA5 global reanalysis from 1940 to 2022, Quarterly Journal of the Royal Meteorological Society, 150, 4014–4048, https://doi.org/10.1002/qj.4803, 2024.

Sousa, P. M., Barriopedro, D., Ramos, A. M., García-Herrera, R., Espírito-Santo, F., and Trigo, R. M.: Saharan air intrusions as a relevant mechanism for Iberian heatwaves: The record breaking events of August 2018 and June 2019, Weather and Climate Extremes, 26, 100 224, https://doi.org/10.1016/j.wace.2019.100224, 2019.

Sprenger, M. and Wernli, H.: The LAGRANTO Lagrangian analysis tool – version 2.0, Geoscientific Model Development, 8, 2569–2586, https://doi.org/10.5194/gmd-8-2569-2015, 2015.

Steinfeld, D. and Pfahl, S.: The role of latent heating in atmospheric blocking dynamics: a global climatology, Climate Dynamics, 53, 6159–6180, https://doi.org/10.1007/s00382-019-04919-6, 2019.

Steinfeld, D., Boettcher, M., Forbes, R., and Pfahl, S.: The sensitivity of atmospheric blocking to upstream latent heating – numerical experiments, Weather and Climate Dynamics, 1, 405–426, https://doi.org/10.5194/wcd-1-405-2020, 2020.

Séchet, G.: Quel temps ! chronique de la météo de 1900 à nos jours, Hermé, Paris, ISBN 978-2-86665-395-8, http://ark.bnf.fr/ark:/12148/cb39174322b, 2004.

Vautard, R., Van Aalst, M., Boucher, O., Drouin, A., Haustein, K., Kreienkamp, F., Van Oldenborgh, G. J., Otto, F. E. L., Ribes, A., Robin, Y., Schneider, M., Soubeyroux, J.-M., Stott, P., Seneviratne, S. I., Vogel, M. M., and Wehner, M.: Human contribution to the record-breaking June and July 2019 heatwaves in Western Europe, Environmental Research Letters, 15, 094 077, https://doi.org/10.1088/1748-9326/aba3d4, 2020.

Vautard, R., Cattiaux, J., Happé, T., Singh, J., Bonnet, R., Cassou, C., Coumou, D., D'Andrea, F., Faranda, D., Fischer, E., Ribes, A., Sippel, S., and Yiou, P.: Heat extremes in Western Europe increasing faster than simulated due to atmospheric circulation trends, Nature Communications, 14, 6803, https://doi.org/10.1038/s41467-023-42143-3, 2023.

Wang, L., Lu, J., Breeden, M. L., Chen, G., Henderson, S. A., Narinesingh, V., Simpson, I. R., Woollings, T., Hu, Y., and Lubis, S. W.: Gaps and ways forward in atmospheric blocking and extreme weather research, Nature Communications, 17, 2873, https://doi.org/10.1038/s41467-026-70487-z, 2026.

Wernli, H. and Davies, H. C.: A Lagrangian-based analysis of extratropical cyclones. I: The method and some applications, Quarterly Journal of the Royal Meteorological Society, 123, 467–489, https://doi.org/10.1002/qj.49712353811, 1997.

Woollings, T., Barriopedro, D., Methven, J., Son, S.-W., Martius, O., Harvey, B., Sillmann, J., Lupo, A. R., and Seneviratne, S.: Blocking and its Response to Climate Change, Current Climate Change Reports, 4, 287–300, https://doi.org/10.1007/s40641-018-0108-z, 2018.

Xu, W., Wu, D., Ciais, P., Wang, Y.-P., Huang, M., Yuan, W., and Liu, J.: Earlier and faster heatwave onset on land under a warming climate, Nature Climate Change, https://doi.org/10.1038/s41558-026-02762-2, 2026.

Zschenderlein, P., Pfahl, S., Wernli, H., and Fink, A. H.: A Lagrangian analysis of upper-tropospheric anticyclones associated with heat waves in Europe, Weather and Climate Dynamics, 1, 191–206, https://doi.org/10.5194/wcd-1-191-2020, 2020.